The Pennsylvania State University

The Graduate School

Mechanical and Nuclear Engineering Department

CARBON DIOXIDE CAPTURE FROM EXHAUST GASES BY AMINE SPRAYS

A Thesis in

Mechanical Engineering

by

Satyajeet M Paranjpe

Submitted in Partial Fulfillment
of the Requirements
for the Degree of

Master of Science

August 2010

The thesis of Satyajeet M Paranjpe was reviewed and approved* by the following:

Professor's Name: Prof. Savas Yavuzkurt
Title(s) : Professor
Thesis Advisor
Chair of Committee

Professor's Name: Prof. Anil Kulkarni
Title(s) : Professor
Thesis Co-Adviser

Professor's Name: Prof H Joseph Sommer III
Title(s) : Professor
Head of the Department of Department or Graduate Program

*Signatures are on file in the Graduate School

ABSTRACT

A new method for carbon dioxide capture is illustrated here without the use of contacting mechanisms like membranes and scrubbers. This study provides a quantitative estimation of how much amine is needed to capture one ton of carbon dioxide, by directly spraying monoethaloamine (MEA) into exhaust gases. First the flow over a sphere is analyzed and the drag coefficient and Nusselt number is compared with published data which matches within 5%. The properties of (MEA) and MEA carbamate are simulated using the Gaussian software which are used for the evaporation and the reaction analysis. In evaporation study, the evaporation of water droplets is analyzed and compared with published data using the discrete phase model (DPM) in FLUENT. The analytical and the CFD results matched within 10%. Amine evaporation model was then analyzed to measure the evaporation from the amine droplets in order to find out the feasibility of this model which shows that the amine droplet evaporation is very low compared to water droplet evaporation due to its low saturation vapor pressure. Finally the reaction is simulated in laminar and turbulent regimes with and without the presence of other exhaust gases like H_2O, N_2, O_2 and CO. Shrinking core model has been used to simulate the reaction. The results prove that the method of CO_2 capture using amine sprays is possible even in practice in turbulent flow regime. This study estimates that for capturing 1 ton of CO_2, 13.6 kg of MEA is required with a MEA droplet size of 300 micrometers.

TABLE OF CONTENTS

LIST OF FIGURES

LIST OF TABLES

Nomenclature

μ= viscosity of the fluid

ρ_p= density of the particle

β = temperature exponent (dimensionless)

Δs = grid spacing near the boundary layer (mm)

dp = diameter of the particle`

Re = relative Reynolds number

u_p = velocity of the particle

u = velocity of the fluid

C_D = drag coefficient

$\dot{m}_p$ = mass flow rate of the particles

Δt = time step

F_{other} = other interaction forces

m_{pin} = mass of the particle on cell entry (kg)

m_{pout} = mass of the particle on cell exit (kg)

Cp_p = heat capacity of the particle (J/kg-K)

H_{pyro} = heat of pyrolysis as volatiles are evolved (J/kg)

T_{pin} = temperature of the particle on cell entry (K)

T_{pout} = temperature of the particle on cell exit (K)

T_{ref} = reference temperature for enthalpy (K)

H_{latref} = latent heat at reference conditions (J/kg)

c_{pg} = heat capacity of gas product species (J/kg-K)

T_{bp} = boiling point temperature (K)

H_{lat} = latent heat at the boiling point temperature (J/kg)

m_p = mass of the particle (kg)

C_p = heat capacity of the particle (J/kg-K)

Ap = surface area of the particle (m2)

T_∞= local temperature of the continuous phase (K)

h^* = convective heat transfer coefficient (W/m2-K)

N_i = molar flux of vapor (kgmol/m^2-s)

k_c = mass transfer coefficient (m/s)

$C_{i;s}$ = vapor concentration at the droplet surface (kgmol/m^3)

$C_{i;\infty}$ = vapor concentration in the bulk gas (kgmol/m^3)

Di,m = diffusion coefficient of vapor in the bulk (m2/s)

Sc = the Schmidt number,

d_p = particle (droplet) diameter

$M_{w,i}$ = molecular weight of species i (kg/kgmol)

m_p = mass of the droplet (kg)

A_p = surface area of the droplet (m^2)

Cj,r = molar concentration of species j in reaction r (kgmol/m^3)

n_{jr} = rate exponent for reactant species j in reaction r

m_{jr} = rate exponent for product species j in reaction r

Ar = pre-exponential factor (consistent units)

E = activation energy for the reaction (J/kgmol)

R = universal gas constant (J/kgmol-K)

Xc = mole fraction of CO_2

Xmc = mole fraction of MEA Carbamate

h = enthaply (J/kg)

njr = rate exponent for reactant species j in reaction r

mjr = rate exponent for product species j in reaction r

t = time (s)

Lp = longitudinal position (m)

ACKNOWLEDGEMENTS

I would like to sincerely thank Prof. Savas Yavuzkurt for being an excellent mentor over the entire course of my MS thesis. His excellent balance of encouragement in the face of difficulty and guidance backed by his indubitable technical knowledge has been wonderful. By far the best aspect has been his ability to get the best out of me by making me thoroughly enjoy my work.

I also sincerely thank Prof. Anil Kulkarni for his inputs and his careful review of my thesis.

I would especially like to thank Mr. Neeraj Kumbhakaran for his invaluable help in Gaussian simulations and chemkin transport program.

I would also like to thank Sushant Dhiman, Aneesh Vadvadgi and Kaushik Joshi for their help in understanding the intricacies of ANSYS/FLUENT. Their constant support has helped me achieve deadlines with ease and confidence.

Chapter 1

Introduction

1.1 Background

Global warming is the one of the major problems commonly faced by everyone today. It is bound to affect each and everyone on this planet no matter where one lives. Global warming is the increase in the average temperature of the earth's near surface air and oceans. This phenomenon was first discovered in 20^{th} century, though green house effect was proposed by Joseph Fourier in 1824 and quantitatively investigated by Svante Arrhenius in 1896[3]. Global warming is the effect of greenhouse effect. Greenhouse effect is the process by which the atmospheric gases absorb and emit infrared radiation in order to keep the earth's lower atmosphere and surface warm. Greenhouse gases emitted by natural processes tend to keep the earth's temperature at about 33 deg Celsius of (59^0 F)[14]. These greenhouse gases are water vapor which contributes to 36% - 70% of the greenhouse effect, carbon dioxide (CO_2) which contributes about 9% - 26%, methane contributes about 4% - 9% and ozone (O_3) which contributes about 4% - 9% [7].

The industrial revolution that began in the beginning of the 20^{th} century sparked an increase in the amount of CO_2 and methane in atmosphere. The concentration of CO_2 and methane has increased by 36% and 148% respectively since 1750 [18]. These levels are much higher than at any time during the last 650,000 years, the period for which reliable data has been extracted from ice cores. The rising CO_2 in the atmosphere means that less amount of infrared radiation is emitted back into the space causing the average temperature of the near earth's lower atmosphere to increase. The effect of global warming is the melting of the polar ice caps which have resulted in increasing the ocean levels posing a severe

danger to the coastal regions of the world. Another effect of global warming is the fact that melting of polar ice caps has resulted in disruption of global fishing industry as well as crop production.

Hence, eliminating the use of fossil fuels for power production and use of alternative renewable energy sources has been sought all over the world. However there are a lot of problems in adopting renewable energy sources. Firstly given the amount of power consumption in the world today and increase in this demand annually the present renewable energy sources cannot satisfy the demand. Hence there has been a lot of research all over the world to increase the power yield of these renewable energy sources. Secondly, the cost of power generation from these renewable sources is much higher than the cost of power generation from fossil fuels. Thirdly, recently it has been estimated that there is about 100 trillion gallons of crude oil reserves in the world and about 847 billion tons of coal reserves in the world. The coal reserves alone will last for about 130 years[22].

Considering all these factors, it is safe to assume that fossil fuels are still going to be a major source in energy production all around the world at least for the next couple of decades. However, one cannot go on emitting CO_2 into the atmosphere at the present rate. So the best possible via media for this problem is to capture carbon dioxide and store it beneath the earth's crust or safely dispose it into the space. As a matter of fact, the major oil companies are in need of carbon dioxide. These companies pump CO_2 into deep hard to reach oil wells, which cause the oil in these wells to rise to the surface thus reducing the cost of oil production.

However, CO_2 capture technology needs some research to be done. The main factor that prevents all the industries adopting the technology is the cost involved in the capture process. One of the main causes for the cost comes from the contacting devices that are used to facilitate the contact between CO_2 and the capturing or absorbing chemical which is usually primary, secondary or tertiary amine solutions

or a mixtures of these. This thesis attempts to capture CO2 from combustion exhaust without the use of the contacting devices, by use of a spray similar to the ones used for SO_2 capture.

Chapter 2

Theory for CO_2 Capture Study

2.1 Capture Chemicals

The most commonly used CO_2 capture chemicals used are amines. Amines can be classified into three types namely primary, secondary and tertiary amines. The main difference between these three types is the number of hydrogen atoms bonded with nitrogen atom. In primary amines the nitrogen in the amino group carries two hydrogen atom while the case of secondary amines the nitrogen carries only one hydrogen atom and in case of tertiary amines there are no hydrogen atoms attached to nitrogen in the amino group. Primary and secondary amines react in a similar way with CO_2 while tertiary amines have a different type of reaction with CO_2, due to the absence of hydrogen atoms attached to nitrogen atom.

2.1.1 Primary amines

The most commonly used primary amine is monoethanolamine (MEA). Its molecular formula is $OHC_2H_4NH_2$. Figure 2.1.1 shows the structure of MEA .

MEA readily reacts with carbon dioxide to form zwitterions which releases a H+ ion which further reacts with either a base or another MEA molecule to form MEAH+. The basic reaction that takes place is as follows[5].

$$OHC_2H_4NH_2 + CO_2 \Longrightarrow OHC_2H_4NHCOO^- + H^+ \quad (2.1)$$

$$H^+ + OHC_2H_4NH_2 \Longrightarrow OHC_2H_4NH_3^+ \quad (2.2)$$

In this reaction the first reaction is the rate determining step while the second reaction is instantaneous.

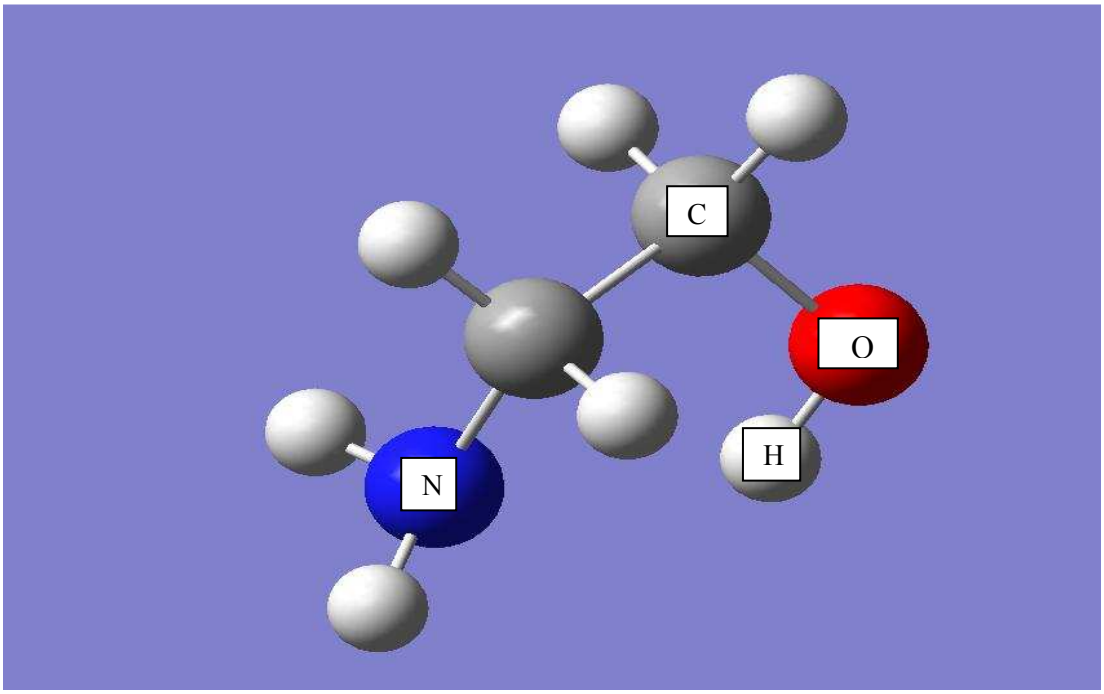

Figure 2.1.1: molecular structure of MEA molecule obtained from Gaussian simulation

2.1.2 Secondary Amines

The most commonly used secondary amine is diethanolamine (DEA). It's molecular formula can be written as $(OHC_2H_4)NH$. DEA also reacts with CO2 readily but the reaction is not as fast as the one with MEA. In this case too zwitterions are formed while the H^+ ion released further reacts with a base of or DEA molecule to form a $DEAH^+$ ion. The reaction is as follows[5].

$$(OHC_2H_4)_2NH + CO_2 \Longrightarrow (OHC_2H_4)_2NCOO^- + H^+ \quad (2.3)$$

$$H^+ + (OHC_2H_4)_2NH \Longrightarrow (OHC_2H_4)_2N\,H_2^+ \quad (2.4)$$

2.1.3 Tertiary Amines

There are many tertiary amines used for the capture process however, triethanolamine (TEA) and methyldiethanolamine (MDEA) are the popular ones.

The molecular formula for TEA is $(OHC_2H_4)_3N$ and that of MDEA is $CH_3N(C_2H_4OH)_2$ [10]. . The molecular structure of MDEA is shown in figure 2.1.2.

Tertiary amines react in a different way than the primary or the secondary amines. In case of tertiary amines, the carbon dioxide capture is done by hydrolysis of water and the amine itself acts as catalyst. Since Tertiary amines do not have any hydrogen attached to the nitrogen atom hence zwitterions cannot be formed.

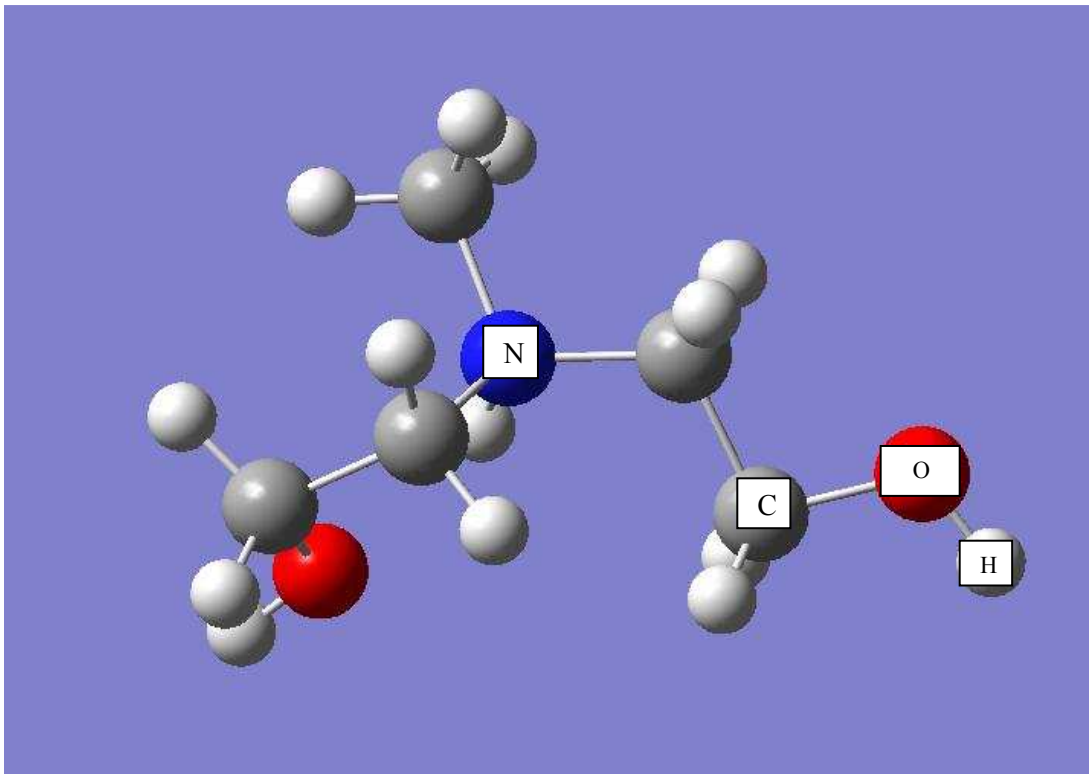

Figure 2.1.2: Molecular structure of MDEA molecule obtained from Gaussian simulation.

2.2 Shrinking Core Model

The figure 2.2.1 helps us visualize the reaction happening on the surface of the amine drop. It is important to note that though the model was developed for solid particles reacting with gas without change in the size of solid particles. This model was validated by studying partially combusted particles of coal. Sections of partially combusted coal particles were analyzed as shown in figure 2.2.1. The blue part inside the particle indicates the unreacted core while the black outer part indicates the reacted material. The same model can be used for reaction between droplets and gaseous phase provided the evaporation from the droplet is zero or negligible.

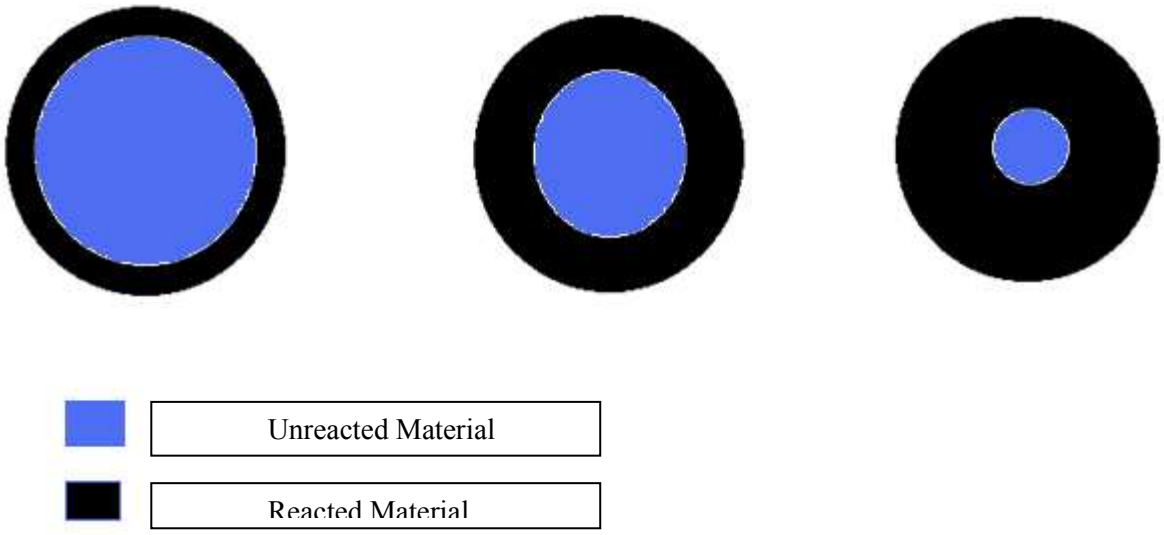

Fig 2.2.1: Shrinking core model shown in stages. [30]

Here the reaction first occurs at the outer skin of the droplets. The zone of the reaction then moves inwards of the drop leaving behind the reacted material. Thus at any time during the process each particle will have the reacted outer part with unreacted core.

The model can be explained in 3 steps [30]:

1) Diffusion of gaseous reactant (CO_2 in this case) through the mixture of gases to the surface of the droplet
2) Diffusion of CO_2 through the layer of reacted material to the surface of the unreacted core.
3) Reaction of CO_2 with the unreacted core containing MEA.

It is evident that at a given time in the process one of these three steps controls the overall process and is the rate determining step. In the case of droplets being injected into an atmosphere of CO_2 only, the first step will be non existent. However as the mole fraction of CO_2 reduces in the gas mixture this resistance becomes more and more predominant.

At the start of the process there is no reacted material, therefore, the second step is non existent. However this resistance increases with time as the layer of reacted material increases. The resistance also depends on the nature of the products produced due to the reaction. In some cases it is noted that even if the thickness of the reacted material increases, the reactant can easily diffuse through the thickness. This usually happens if the reaction is slow so that reaction now becomes the rate determining step.

The model can be used for the present case as the rate of evaporation of amine drops is very slow compared to the amount of time it takes for the amine drops to travel through the capture chamber. This is attributed to their low saturation vapor pressure which is discussed ahead in the amine droplet evaporation study.

The figure below shows the overall process of a single amine droplet.

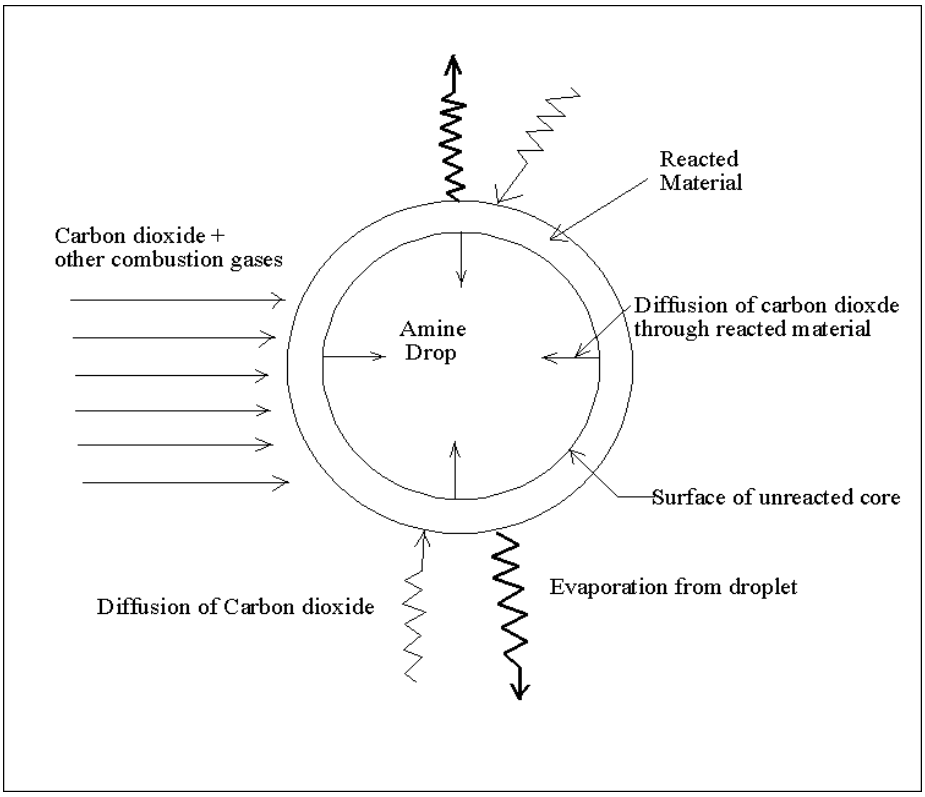

Fig 2.2.2 : Showing different processes taking places around and in an amine droplet during CO_2 Capture

It is important to note that other combustion gases like N_2,O_2 and H_2O do not react with amines. Hence amines are favorable capture chemicals [6].

Chapter 3

Qualification of CFD Model

The first objective before the evaporation and reaction simulation was to simulate the flow over a sphere, find out the Nusselt number and drag coefficient and match those results with the published data. Also grid sensitivity study was carried out to find out the optimum grid specifications.

3.1 Drag Coefficient Calculations

The nature of flow across a sphere strongly affects the drag coefficient C_D. Both the friction and pressure can be significant. The high pressure in the vicinity of the stagnation point and the low pressure in the wake region produce a net force on the body in the direction of the flow. The drag force is primarily due to friction drag at low Reynolds number ($Re < 10$) and the pressure drag at high Reynolds number ($Re > 5000$). Both are significant at intermediate Reynolds number.

The figure below gives drag coefficients for a smooth sphere and cylinder at different Reynolds numbers.

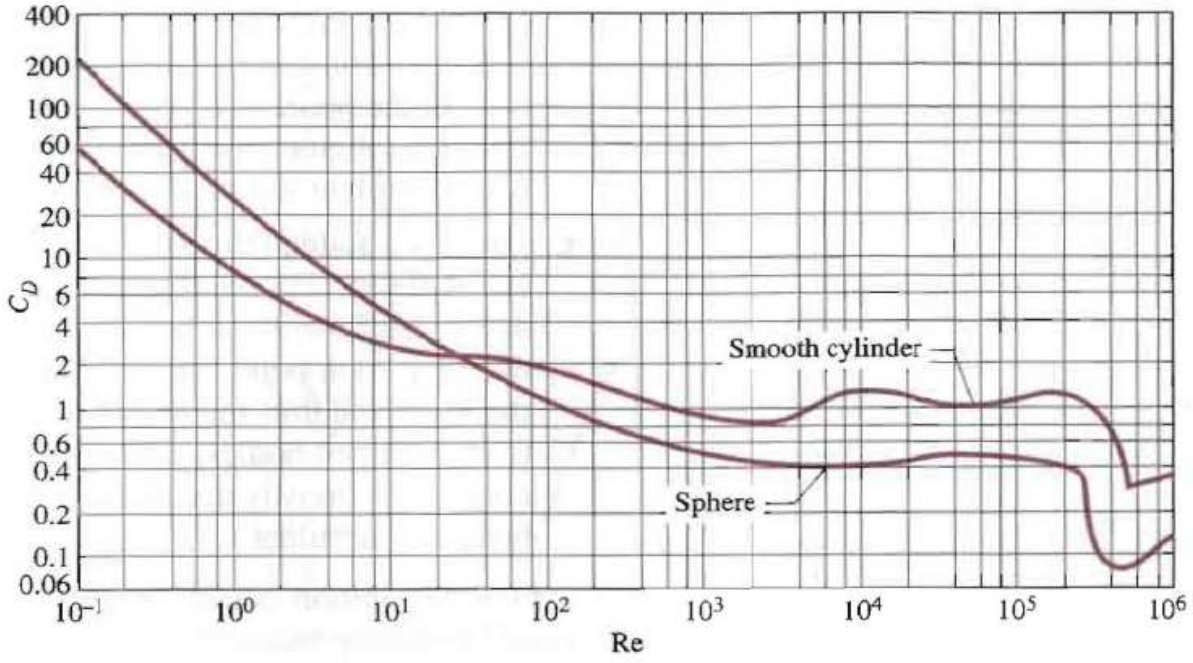

Fig 3.1.1 : Drag Coefficient as a function of Reynolds number for a sphere and cylinder [31].

The drag coefficient obtained from FLUENT simulation is 2.96 which matches closely with the above figure which predicts it to be around 2.8 at a Re 29.51. This is a deviation of 5% from the actual value predicted by the plot above.

3.2 Grid Generation:

Here the grid generated was a simple one. We had a sphere inside a cylinder. Due to symmetry, only half of the cylinder and sphere was meshed. A boundary layer was generated near the sphere to capture the boundary layer effects. The dimensions of the domain were as follows:

Diameter of drop: 3×10^{-4} m

Diameter of domain: 6×10^{-4} m

Length of domain: 12×10^{-4} m

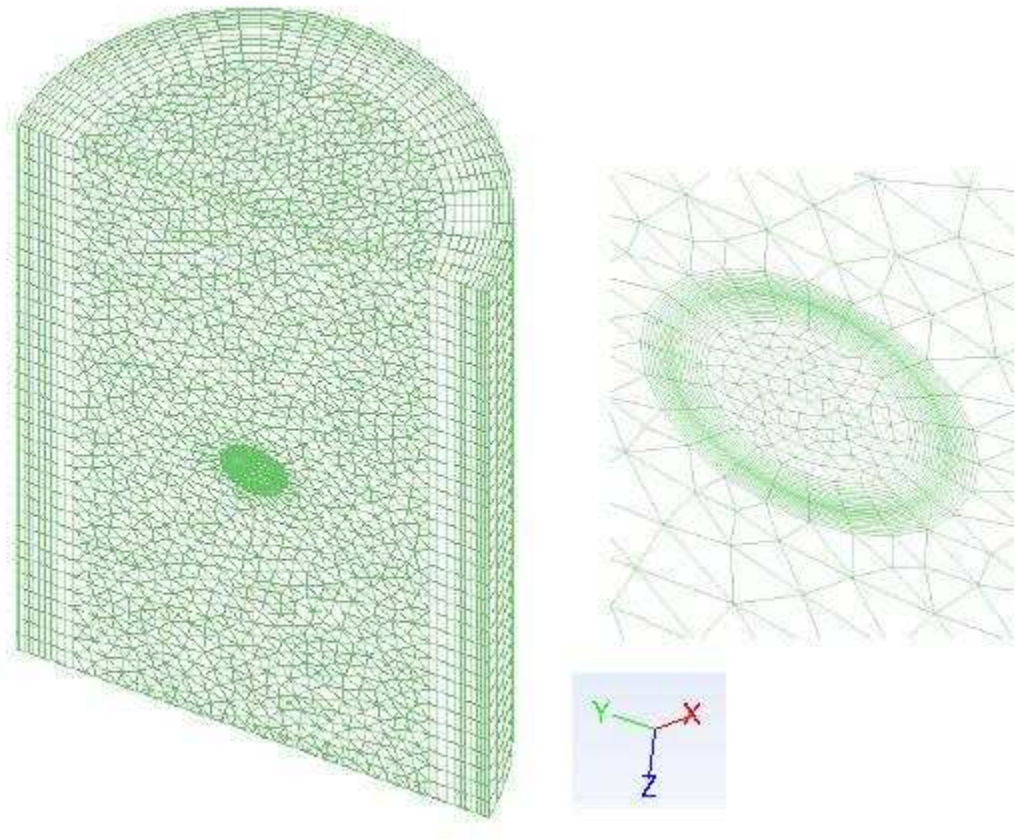

Fig 3.2.1: Grid of the domain with the droplet also showing the boundary layer grid

3.3Nusselt Number Calculations

Flow across a sphere generally involves flow separation which is difficult to handle analytically. Hence such flows must be studied experimentally or numerically.

For flow over a sphere the following correlation is given by Whitaker [31]:

$$N_D = \frac{hD}{k} = 2 + [0.4Re^{1/2} + 0.06Re^{2/3}]\, Pr^{0.04} \left[\frac{\mu_\infty}{\mu}\right]^{0.25} \qquad (3.2.1)$$

The equation is valid for $3.5 \leq Re \leq 80{,}000$ and $0.7 \leq Pr \leq 380$. The fluid properties are evaluated at the free stream temperature T_∞ , except for μ which is evaluated at surface temperature T_s.

The fluid used was air with an approach velocity of 2.5 m/s and a temperature of 313 K. The temperature of the drop is 300 K which gives a Re of 29.51 and Pr of 0.72. hence we can use the above correlation to compare it with the Nusselt number obtained from FLUENT simulation.

The convective heat transfer co-efficient obtained from FLUENT was 603.84 W/m^2k and the corresponding Nusselt number is Nu = 4.5197. While the Nusselt number obtained from the correlation is Nu = 4.5436. This is a 1% deviation from the formula.

3.4 Grid Sensitivity Study

To optimize grid specifications a grid sensitivity study was carried out to see the effect of change of grid on Nusselt number calculations. The grid spacing near the boundary layer was changed. The results were as follows

Δs spacing (mm)	h^* from simulation (W/m^2k)	Nu from simulation
0.075	497.93	4.52
0.05	485.95	4.41
0.03	478.70	4.34

Table:3.4.1 : variation of Nusselt number with change in grid dimensions

After grid spacing of 0.03 mm the change in the value of h^* was less than 1%, hence 0.03 mm was the grid spacing used for further study. It should be noted that as the grid spacing is reduced the Nusselt number is also reduced but it deviates away from the empirical value of 4.5436. However, Whitaker indicated that the correlation is not very accurate and results that deviate to about 15% are acceptable [31].

Chapter 4

Simulating Properties of Species using Gaussian Software

In order to simulate evaporation or reaction for the amines finding the properties of MEA and MEA carbamate and finding the dependence of these properties on temperature was very important. For this purpose, the Gaussian software was used.

Gaussian is a molecular dynamics software in which one can build the molecule of choice and the software then simulates the properties of the molecule. Gaussian however, only gives the basic properties. The behavior of these properties with respect to changing temperature was found by using the CHEMKIN transport program [20].

The CHEMKIN transport program gave the variation of Cp with temperature. The values of Cp so obtained were then fitted to a curve in Matlab and the function so obtained was used to find the variation of enthalpy and entropy with temperature.

The process is illustrated below. First the properties of MEA were found and then the properties of MEA carbamate were found out.

4.1 Simulating Properties of MEA

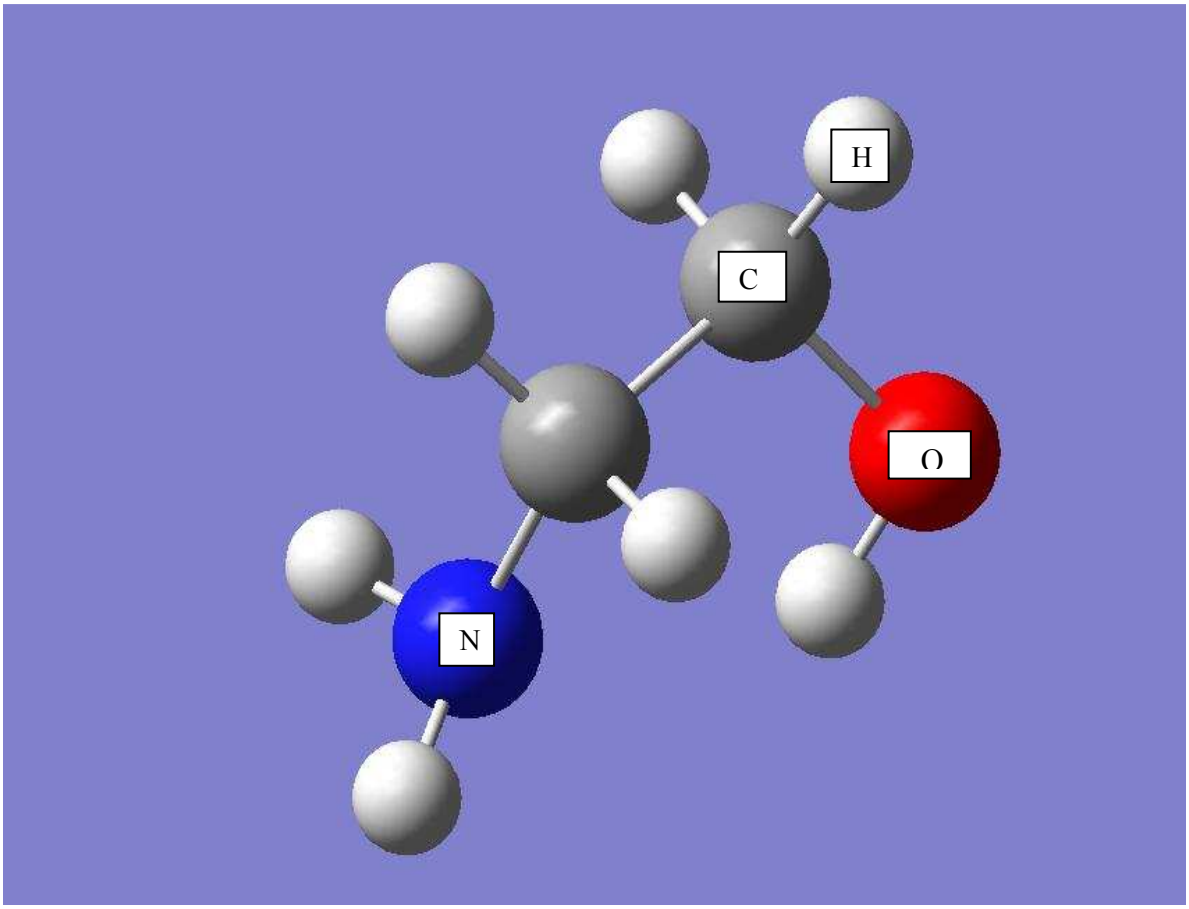

Fig 4.1.1:Stable MEA molecule

The MEA molecule shown above is the final stable molecule obtained by Gaussain after simulation. The different colors used to indicate different atoms are as per the molecular dynamics convention. The white balls indicate the hydrogen atoms, the grey balls indicate the carbon atoms, red ball stands for oxygen atom while the blue ball stands for nitrogen. The same convention is followed for MEA carbamate . The meaning of the word “stable” MEA molecule means that the angles between the bonds have the least energy as obtained at standard temperature and pressure. It is important to note the option selected for this simulation is that of “optimum + frequency” in Gaussian. This option is

particularly useful in finding the Cp of the molecule. However the simulation does not provide the variation of Cp with temperature.

In order to find this, the CHEMKIN transport program was used. The variation of Cp with temperature was found for a temperature range of 100 K to 1000 K. The table 4.1.1 below shows the output of the CHEMKIN transport program.

T (K)	Cp (J/mol.K)
100.00	41.37
200.00	57.70
273.00	70.75
283.00	72.65
293.00	74.58
298.15	75.57
300.00	75.93
303.00	76.52
313.00	78.48
323.00	80.45
333.00	82.43
343.00	84.41
400.00	95.67
500.00	114.25
600.00	130.52
700.00	144.47
800.00	156.49
900.00	166.94
1000.00	176.09

Table 4.1.1: Variation of specific heat with temperature for MEA

The values so obtained were fitted onto a curve using Matlab. A 3rd degree polynomial was found to be the best fit.

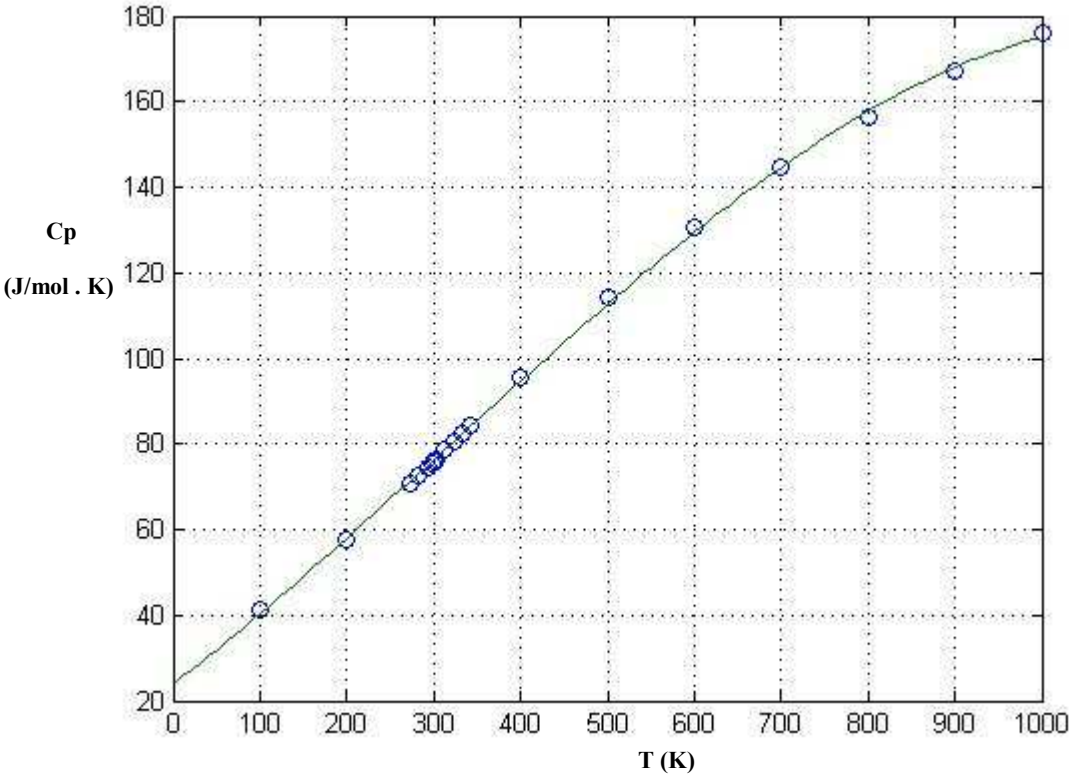

Fig 4.1.2: Variation of Specific Heat of MEA with temperature.

The equation so obtained is given below [32][2].

$$Cp = 23.8952 + 0.1566\,T + 0.0001\,T^2 \qquad (4.1)$$

Division by Universal gas constant R (8.314 J/mol.k) gives the following dimensionless equation

$$\frac{Cp}{R} = 2.8873927 + 0.018834629\,T + 1.2027222E\text{-}05\,T^2 \qquad (4.2)$$

The equation 4.1.2 was then used to find the equation for enthalpy as a function of temperature.

For the purpose the following formula was used [32].

$$\frac{h}{R} = \frac{h_{f298}}{R} + \int_{298}^{T} \frac{Cp}{R}\, dT \tag{4.3}$$

Here, $h_{f\,298}$ is the enthalpy of formation of MEA which is -280.9 kJ/mol [11]. Substituting the value of C_p/R in the above equation, we get the following equation of enthalpy as a function of temperature,

$$\frac{h}{RT} = 2.8739287 + \frac{0.018834629}{2} T + \frac{1.2027222e{-}05}{3} T^2 - \frac{35583.2868}{T} \tag{4.4}$$

The equation 4.1.2 was also used to find the equation of entropy as a function of temperature. For this purpose the following formula was used [32],

$$\frac{s}{R} = \int_{298}^{T} \frac{Cp}{RT}\, dT \tag{4.5}$$

Substituting the value of C_p/R in the above equation, we get the following equation of entropy as a function of temperature,

$$\frac{s}{R} = 2.878739287 \ln T + 0.018834629\, T + \frac{1.2027222e{-}05}{2} T^2 - 22.5197926 \tag{4.6}$$

4.2 Simulating Properties of MEA Carbamate:

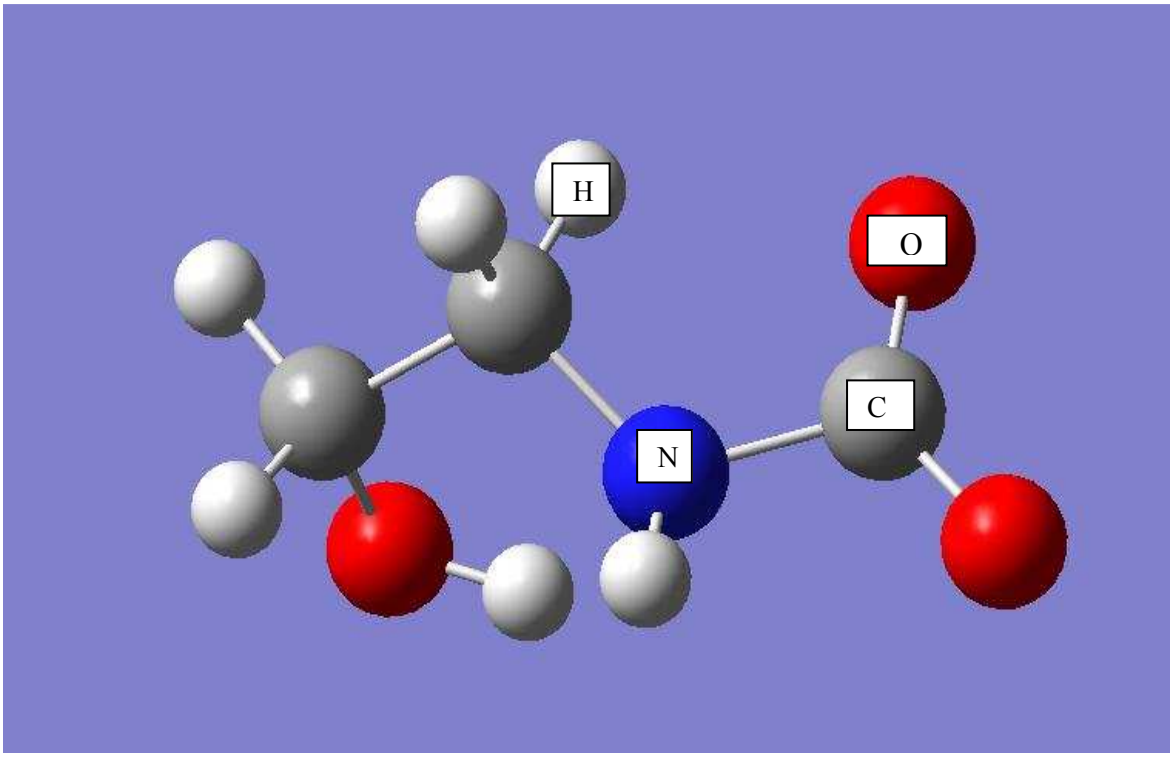

Fig 4.2.1: Stable molecular structure of MEA carbamate.

Here, the different colors of the atoms follow the molecular dynamics convention as mentioned in the above section. It is important to note that the MEA carbamate carries a negative charge. Hence while simulating the molecule in Gaussian, apart from choosing the "optimum + frequency" option we also have to specify the charge on the molecule. In Gaussian, the charge is specified as follows: Neutral molecule is denoted by number 0, while positive or negative charge is denoted by +1 and -1 respectively. As specified before, the word "stable" means that the molecule has optimum bond angles in ground state as one would find at standard temperature and pressure.

As discussed before the output of the Gaussian simulation was fed to the CHEMKIN transport program to find the variation of Cp with temperature in a range of 100 K to 1000 K.

T (K)	Cp (J/mol.K)
100.00	54.70
200.00	78.07
273.00	95.85
283.00	98.37
293.00	100.90
298.15	102.21
300.00	102.69
303.00	103.45
313.00	106.00
323.00	108.56
333.00	111.12
343.00	113.68
400.00	128.08
500.00	151.53
600.00	171.80
700.00	188.91
800.00	203.35
900.00	215.60
1000.00	226.06

Table 4.2.1: Variation of specific heat with temperature for MEA Carbamate.

The values so obtained were fitted onto a curve using Matlab. A 3rd degree polynomial was found to be the best fit.

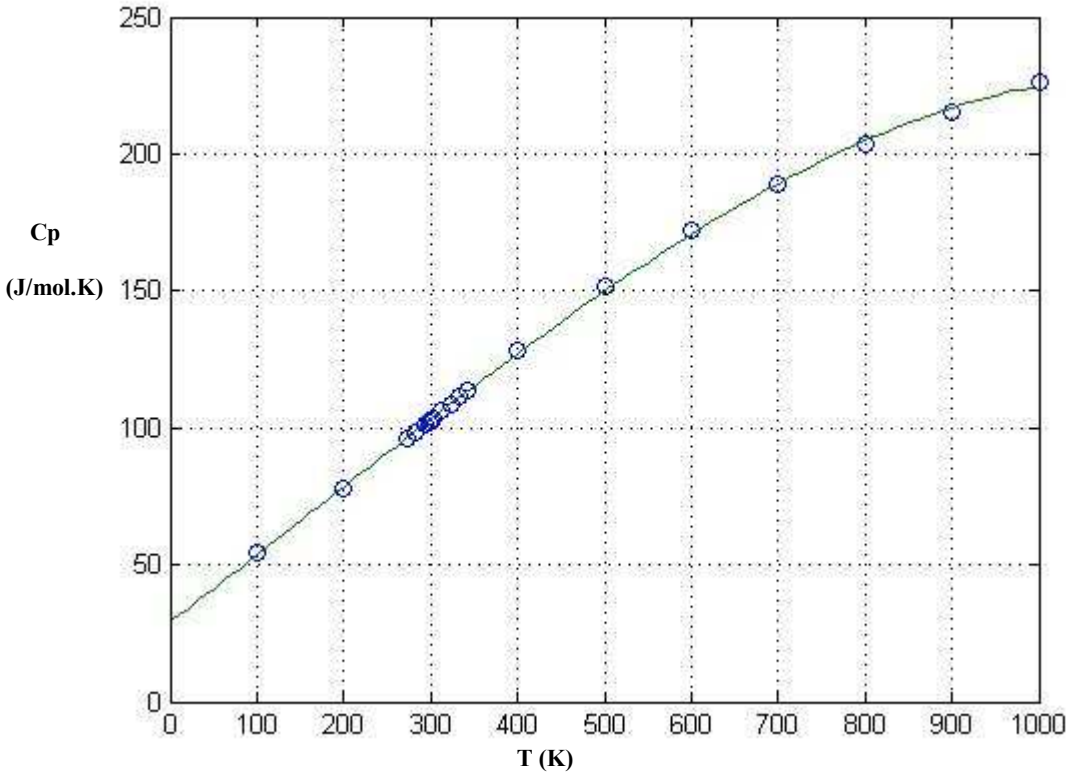

Fig 4.2.2: Variation of specific heat of MEA Carbamate with temperature

Following the same process as shown for MEA , we obtain the following correlations for MEA carbamate [32][11][2].

$$\frac{Cp}{R} = 2.9684987 + 0.01842570\ T + 1.20272219E\text{-}05\ T^2 \qquad (4.8)$$

$$\frac{h}{RT} = 2.9684987 + \frac{0.01842570}{2} T + \frac{1.20272219e-05}{3} T^2 - \frac{40223.7919}{T} \qquad (4.10)$$

$$\frac{s}{R} = 2.9684987 \ln T + 0.01842570\ T + \frac{1.20272219e-05}{2} T^2 - 22.936706 \qquad (4.12)$$

4.3 Material Property Program in FLUENT

Following the guideline mentioned above, the properties of MEA and MEA carbamate were calculated and entered into FLUENT. However, this time the properties were added directly to the FLUENT property database program prop.scm.

The following is the piece of code that was entered in FLUENT program prop.scm [8][3][2].

```
(monoethanolamine
 (fluid combustion-particle solid)
 (chemical-formula . hoc2h4nh2)
 (specific-heat (polynomial piecewise-polynomial (100 1000 2.9684987    0.01842570 1.2027222e-05 0 0) (1000 5000
2.9684987 0.01842570 1.2027222e-05 0 0)))
 (molecular-weight (constant . 61.08))
 (formation-enthalpy (constant . -2.809e+08))
 (reference-temperature (constant . 298))
 (formation-entropy (constant . 187240.185))
 (density (constant . 1016))
 (thermal-conductivity (constant . 0.2918))
 (latent-heat (constant . 837000))
 )
```

Chapter 5

Discrete Phase Model (DPM) in FLUENT

To simulate the spraying of amines into the combustion exhaust, the discrete phase model (DPM) was used. The DPM model in FLUENT is used to simulate a discrete secondary phase in the Langrangian frame of reference [33]. The secondary phase can be droplets or small solid particles. FLUENT calculates the trajectories of these injections and also computes the heat and mass transfer to and from the secondary phase. The DPM model is very useful for modeling

- Heating or cooling of discrete phase,
- Boiling or evaporation of liquid droplets,
- Combusting particles. (It can also simulate volatile evolution and char combustion to simulate coal combustions), and ,
- Droplet break up and coalescence .

These modeling capabilities allow FLUENT to simulate a wide range of discrete phase problems including particle separation and classification, spray drying, aerosol dispersion, bubble stirring of liquids, liquid fuel combustion, and coal combustion.

The DPM allows the user to include various forces which might act on the particles like thermophoretic force, Brownian force, and Saffman's Lift force. It also allows for laminar as well as turbulent dispersion of particles in the domain. The DPM model was used in this study for simulating the evaporation of water droplets initially and later to simulate the evaporation from amine droplet.

5.2 Particle Force Balance

FLUENT predicts the trajectory of a discrete phase particle (or droplet or bubble) by integrating the force balance on the particle, which is written in a Lagrangian reference frame. This force balance equates the particle inertia with the forces acting on the particle [33] and can be written (for the x direction in Cartesian coordinates) as

$$\frac{du_p}{dt} = F_D\,(u - up) + \frac{gx\,(\rho_p - \rho)}{\rho} + F_x \tag{5.1}$$

where F_x is an additional acceleration (force/unit particle mass) term, $F_D(u - up)$ is the drag force per unit particle mass and

$$F_D = \frac{18\mu\, C_D}{\rho_p\ d_p^2}\ \frac{Re}{24} \tag{5.2}$$

Here, u is the fluid phase velocity, u_p is the particle velocity, μ is the molecular viscosity of the fluid, ρ is the fluid density, ρ_p is the density of the particle, and d_p is the particle diameter. Re is the relative Reynolds number, which is defined as [33],

$$Re = \frac{\rho\ d_p\,|u_p - u|}{\mu} \tag{5.3}$$

5.3 Momentum Exchange

The momentum transfer from the continuous phase to the discrete phase is computed by examining the change in momentum of a particle as it passes through each control volume in the FLUENT model. This momentum change is computed as

$$F_D = \sum \left(\frac{18\,\mu\, C_D\, Re}{\rho_p\, d_p^2\, 24} \left(u_p - u\right) + F_{other} \right) . \dot{m}_p\, \Delta t \qquad (5.4)$$

This momentum exchange appears as a momentum sink in the continuous phase momentum balance in subsequent calculations of the continuous phase flow field.

5.4 Heat Exchange

The heat transfer from the continuous phase to the discrete phase is computed by examining the change in thermal energy of a particle as it passes through each control volume in the FLUENT model. In the absence of a chemical reaction (i.e., for all particle rules except Rule 5) the heat exchange is computed as [33]

$$Q = (m_{pin} - m_{pout}) [- H_{latref} + H_{pyro}] - m_{pout} \int_{T_{ref}}^{T_{pout}} Cp_p\, dt +$$

$$+ m_{pin} \int_{T_{ref}}^{T_{pin}} Cp_p\, dt \qquad (5.5)$$

The latent heat at the reference conditions H_{latref} for droplet particles is computed as the difference of the liquid and gas standard formation enthalpies, and can be related to the latent heat at the boiling point as follows:

$$H_{latref} = H_{lat} - \int_{T_{ref}}^{T_{bp}} Cp_g \, dt + \int_{T_{ref}}^{T_{bp}} Cp_p \, dt \quad (5.6)$$

For the volatile part of the combusting particles, some constraints are applied to ensure that the enthalpy source terms do not depend on the particle history. The formulation should be consistent with the mixing of two gas streams, one consisting of the fluid and the other consisting of the volatiles. Hence H_{latref} is derived by applying a correction to H_{lat}, which accounts for different heat capacities in the particle and gaseous phase:

$$H_{latref} = H_{lat} - \int_{T_{ref}}^{T_{p,init}} Cp_g \, dt + \int_{T_{ref}}^{T_{p,init}} Cp_p \, dt \quad (5.7)$$

5.5 Mass Exchange

The mass transfer from the discrete phase to the continuous phase is computed by examining the change in mass of a particle as it passes through each control volume in the FLUENT model. The mass change is computed simply as

$$M = \frac{\Delta m_p}{m_{p,0}} \dot{m}_{p,0} \quad (5.8)$$

This mass exchange appears as a source of mass in the continuous phase continuity equation and as a source of a chemical species defined by you. The mass sources are included in any subsequent calculations of the continuous phase flow field

5.6 Under-Relaxation of the Interphase Exchange Terms

Note that the interphase exchange of momentum, heat, and mass is under-relaxed during the calculation, so that

$$F_{new} = F_{old} + \alpha(F_{calculated} - F_{old}) \quad (5.9)$$

$$Q_{new} = Q_{old} + \alpha(Q_{calculated} - Q_{old}) \quad (5.10)$$

$$M_{new} = M_{old} + \alpha(M_{calculated} - M_{old}) \quad (5.11)$$

where α is the under-relaxation factor for particles/droplets that one can set in the "Solution Controls" panel.

5.7 DPM Particle types in FLUENT

The laws that you activate depend upon the particle type that you select. In the Set

Particle Type	Description	Rules Activated
Inert	inert/heating or cooling	1, 6
Droplet	heating/evaporation/ boiling	1, 2, 3, 6
Combusting	heating; evolution of volatiles/swelling;	1, 4, 5, 6

	heterogeneous surface reaction	
Multicomponent	multicomponent droplets/particles	7

Table 5.7.1: Types of DPM particles

Injection Properties panel you will specify the Particle Type, and FLUENT will use a given set of heat and mass transfer laws for the chosen type. All particle types have predefined sequences of physical laws as shown in the table below [33]:

5.8 Inert Heating or Cooling

The inert heating or cooling laws (Rules 1 and 6) are applied when the particle temperature is less than the vaporization temperature, T_{vap}, and after the volatile fraction, fv;0, of a particle has been consumed. These conditions may be written

as

\

Rule 1: $$T_p < T_{vap} \quad (5.12)$$

Rule 6: $$m_p \leq (1 - fv;0)\, m_p;0 \quad (5.13)$$

Where T_p is the particle temperature, $m_p;0$ is the initial mass of the particle, and m_p is its current mass. Rule 1 is applied until the temperature of the particle/droplet reaches the vaporization temperature. At this point a noninert particle/droplet may proceed to obey one of the mass-transfer rules (2, 3, 4,

and/or 5), returning to rule 6 when the volatile portion of the particle/droplet has been consumed. (Note that the vaporization temperature, T_{vap}, is an arbitrary modeling constant used to define the onset of the vaporization/boiling/volatilization laws.) When using rule 1 or rule 6, FLUENT uses a simple heat balance to relate the particle temperature, $T_p(t)$, to the convective heat transfer .

$$m_p C_p \frac{dT_p}{dt} = hA_p\left(T_\infty - T_p\right) \tag{5.14}$$

5.9 Droplet Vaporization

Rule 2 is applied to predict the vaporization from a discrete phase droplet [33]. Rule 2 is initiated when the temperature of the droplet reaches the vaporization temperature, T_{vap}, and continues until the droplet reaches the boiling point, T_{bp}, or until the droplet's volatile fraction is completely consumed:

$$T_p < T_{bp} \tag{5.15}$$

$$m_p > (1 - fv;0)\, m_p;0 \tag{5.16}$$

The onset of the vaporization rule is determined by the setting of T_{vap}, a modeling parameter that has no physical significance. Note that once vaporization is initiated (by the droplet reaching this threshold temperature), it will continue to vaporize even if the droplet temperature falls below T_{vap}. Vaporization will be halted only if the droplet temperature falls below the dew point. In such cases, the droplet will remain in rule 2 but no evaporation will be predicted.

5.10 Mass transfer during droplet vaporization

During rule 2, the rate of vaporization is governed by gradient diffusion, with the flux of droplet vapor into the gas phase related to the gradient of the vapor concentration between the droplet surface and the bulk gas:

$$N_i = k_c (C_{i,s} - C_{i,\infty}) \quad (5.17)$$

FLUENT's vaporization law assumes that Ni is positive (evaporation). If conditions exist in which N_i is negative (i.e., the droplet temperature falls below the dew point and condensation conditions exist), FLUENT treats the droplet as inert (N_i = 0:0). The concentration of vapor at the droplet surface is evaluated by assuming that the partial pressure of vapor at the interface is equal to the saturated vapor pressure, p_{sat}, at the particle droplet temperature, T_p:

$$C_{i,s} = \frac{P_{sat}(T_p)}{RT_p} \quad (5.18)$$

Where, R is universal gas constant.

The concentration of vapor in the bulk gas is known from solution of the transport equation for species i :

$$C_{i,\infty} = X_i \frac{p}{RT_\infty} \quad (5.19)$$

where X_i is the local bulk mole fraction of species i, p is the local absolute pressure, and T_1 is the local bulk temperature in the gas. The mass transfer coefficient in Equation 22.9-20 is calculated from the Sherwood number correlation;

The mass of the droplet is reduced according to

$$m_p(t + \Delta t) = m_p(t) - N_i A_p M_{w,I} \Delta t \quad (5.21)$$

5.11 Discrete Phase Model (DPM) Boundary Conditions

When a particle strikes a boundary face, one of several contingencies may arise:

- The particle may be reflected via an elastic or inelastic collision;
- The particle may escape through the boundary. The particle is lost from the calculation at the point where it impacts the boundary;
- The particle may be trapped at the wall. Nonvolatile material is lost from the calculation at the point of impact with the boundary; volatile material present in the particle or droplet is released to the vapor phase at this point;
- The particle may pass through an internal boundary zone, such as radiator or porous jump;
- The particle may slide along the wall, depending on particle properties and impact angle.

5.12 Interaction with Continuous Phase:

In order that the discrete phase interacts (i.e., exchanges mass, momentum, and/or energy) with the continuous phase, the" *Interaction with the Continuous Phase"* option was enabled [33]. An input for the" *Number of Continuous Phase Iterations per DPM Iteration"* allows us to control the frequency

at which the particles are tracked and the DPM sources are updated. For steady-state simulations, increasing the Number of Continuous Phase Iterations per DPM Iteration will increase stability but requires more iterations to converge.

5.13 Parameter Tracking for the Discrete Phase Model

We have two parameters to control the time integration of particle trajectory equations:

- Length scale / step length factor

  This factor is used to set the time step for integration within each control volume;

- the maximum number of time steps

  This factor is used to abort trajectory calculations when the particle never exits the flow domain.

Max. Number Of Steps is the maximum number of time steps used to compute a single particle trajectory. When the maximum number of steps is exceeded, FLUENT abandons the trajectory calculation for the current particle injection and reports the trajectory fate as “incomplete".
Length Scale controls the integration time step size used to integrate the equations of motion for the particle. The integration time step is computed by FLUENT based on a specified length scale L, and the velocity of the particle (u_p) and of the continuous phase (u_c)[33]:

$$\Delta t = \frac{L}{u_p + u_c} \tag{5.22}$$

L is proportional to the integration time step and is equivalent to the distance that the particle will travel before its motion equations are solved again and its trajectory is updated. A smaller value for the Length Scale increases the accuracy of the trajectory and heat/mass transfer calculations for the discrete phase.

5.14 Type of Injection

There are different ways by which we can inject the secondary discrete phase into the domain. We can also specify the position in the domain where we want to inject the discrete phase. FLUENT provides 11 different types of injections

- single,
- group,
- cone (only in 3D),
- solid-cone (only in 3D),
- surface,
- plain-orifice atomizer,
- pressure-swirl atomizer,
- at-fan-atomizer,
- air-blast-atomizer,
- effervescent-atomizer and
- file

In our this study, solid cone injection is used for the water droplet evaporation and amine droplet evaporation study.

Various inputs are required for the solid cone injection. They are as follows:

1. Position of the point in the domain where the discrete phase is to be injected
2. Initial diameter of the injected droplets
3. Initial temperature of the droplets at the time of injection.

4. X,Y, and Z components of the vetor defining the cone's axis
5. Injection velocity of the discrete phase
6. half angle θ of the hollow spray cone
7. A nonzero inner radius can be specified to model injectors. The particles will be distributed about the axis with the specified radius.

Chapter 6

Water Droplet Evaporation

The main aim of the water droplet evaporation study is to make sure that the domain used and the DPM model works with each other. However, there are few more reasons which justify the study of water droplet evaporation by DPM model. One of the reasons is that in industries water is used as a solvent to make amine solutions. So if an amine solution is used in practice, what is the rate at which water from the solution evaporates? This study is also a precursor to the study of amine droplet evaporation. One of the important questions this study will try an answer how feasible, from engineering point of view, is the approach of carbon dioxide capture by direct rapid mixing applicable to tertiary amines like TEA and MDEA.

6.1 Initial Process

The grid for the DPM model was made in Gambit. The grid is simple box of dimensions 20 mm X 20mm X60 mm. The initial water droplet evaporation study was done by injecting a single particle into the domain at a specified point and in a direction opposite to the flow to increase the mass flow rate due to increased relative velocity. The study later included the study of multiple water droplets injected in the domain at a specified point to simulate the behavior of a typical industrial atomizer. For the multiple drop evaporation simulation, the drops were injected in a conical fashion the inputs of which will be defined later.

It was soon realized that the domain length of 60mm is short as compared to the domain cross section of 20mm X 20 mm. This was made evident from the fact that when the DPM simulation was run, a lot of cells in the outlet of the domain had reversed flow.

To counter this problem, the domain length was increased from 60 mm to 160 mm. This solved the issue of reversed flow at the outlet boundary.

6.2 Discrete Phase Model Inputs

The DPM model inputs shown here are the inputs that pertain to the domain 20 mm X 20 mm X 160 mm. As I have indicated before, the inputs given below are for a single particle injected into the domain.

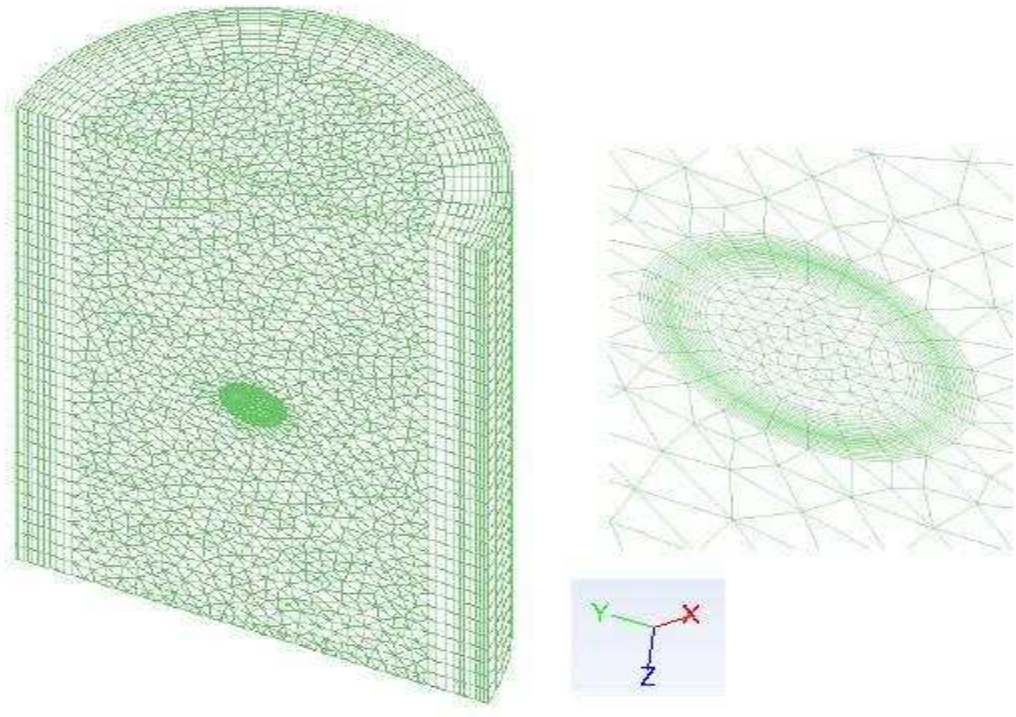

Fig 6.2.1: Domain along with boundary layer grid and axes.

Position:

X axis (mm)	Y axis (mm)	Z axis (mm)
10	10	145

Table 6.2.1: DPM position inputs

Velocity:

X velocity (m/s)	Y velocity (m/s)	Z velocity (m/s)
0	0	-1

Table 6.2.2: DPM Velocity inputs

Diameter: 90 micrometer (90 X 10^{-6} m)

Temperature: 300 K

The Z direction is the longitudinal direction of the domain. The negative Z velocity of the injected particle indicates that the particle is being injected in a direction opposite to the direction of the flow.

One important thing to note here is that in commercial CO_2 capture systems the temperature inside the system is about 313 K with the amine solution being at about the room temperature. The exhaust gases are cooled to the temperature of about 313 K before carbon capture is made possible [16]. The reason for this is that the compounds that are formed during the carbon capture process are very unstable at elevated temperatures. In fact, heating the products is an integral part of the regeneration process.

However, in this case we have used the ambient temperature a 673 k (400 deg C). The reason for this is the fact that we want to compare our results with established water droplet evaporation data. The results of the simulation were compared with the published data on spray evaporative cooling [29] .

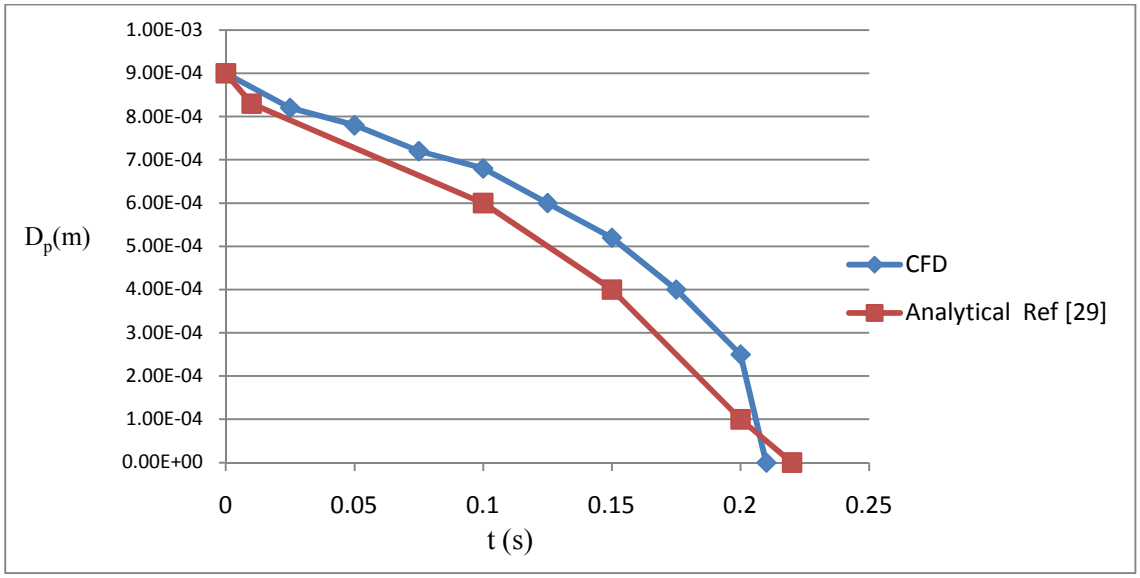

Fig 6.2.2: variation of droplet diameter with time obtained from FLUENT simulation and ref [29]

The comparison between the plots above show that the analytical model used in the paper agrees to the simulation output within 10%.

6.3 Amine Droplet Evaporation Study

Before proceeding with reaction simulation it is important to check the loss of MEA due to evaporation. For this purpose, evaporation study of MEA is done. MEA was injected into domain with the same parameters of water evaporation but the properties of MEA were incorporated in FLUENT DPM simulation which was obtained from Gaussian simulation.

The saturation vapor pressure of MEA is 25 Pa at 293K. Saturation vapor pressure is inversely proportional to the volatility of a liquid. For example the saturation vapor pressure of water at 293 K is 2330 Pa [14]. Hence water evaporates easily.

The above values show that the saturation vapor pressure of MEA is very low as compared to water. Hence, the evaporation of MEA will be very low as compared to water. The same was observed with DPM simulation of MEA .

For the DPM simulation, the MEA droplets were injected in the same place where the water droplets were injected having the same velocity. With water, complete evaporation was obtained with $1x10^4$ DPM time steps with a length scale parameter of 5. However, with MEA the total DPM time steps used were $1 x10^8$ with a length scale parameter of 5. Even at such high number of time steps the particle tracking in DPM showed the results as "incomplete" which means that even such high number of time steps were not enough to completely evaporate the amine droplets. Such high number of time steps is enough for the amine droplets to travel through the capture chamber and finally end up in the collection chamber. Though FLUENT allows maximum time steps as $10 x10^9$, there is no need to increases the time steps as the total time that a droplet has to capture CO_2 is much less than that.

The evaporation also depends on the relative velocity between droplet and gas flow. However increasing the gas flow velocity is not possible as the relative velocity has to be less than the terminal velocity of the falling droplet to avoid loss of MEA to atmosphere.

Chapter 7

Carbon Dioxide Capture Study

After understanding the evaporation study for water droplets and amine droplets and the way the code works, CO_2 capture study with MEA spray was done. For the reaction analysis, simulation of the reaction in the laminar regime as well as the turbulent regime and comparison between them was done. FLUENT can model the mixing and transport of chemical species by solving conservation equations describing convection, diffusion, and reaction sources for each component species. Multiple simultaneous chemical reactions can be modeled, with reactions occurring in the bulk phase (volumetric reactions) and/or on wall or particle surfaces, and in the porous region.

7.1 Theory

In order to solve conservation equations for chemical species, FLUENT predicts the local mass fraction of each species, Y_i, through the solution of a convection-diffusion \equation for the i^{th} species [15]. This conservation equation takes the following general form:

$$\frac{\partial}{\partial t}(\rho Y_i) + \Delta (\rho Y_i \bar{u}) = \Delta . J_i + R_i + S_i \qquad (7.1)$$

Where, R_i is the net rate of production of species i by chemical reaction (described later in this section) and S_i is the rate of creation by addition from the dispersed phase plus any user-defined sources. An equation of this form will be solved for N-1 species where N is the total number of fluid phase chemical species present in the system. Since the mass fraction of the species must sum to unity, the N^{th} mass fraction is determined as one minus the sum of the N-1 solved mass fractions.

7.2 Reaction in Laminar Regime

Initially the reaction was simulated in the laminar regime in order to simulate the reaction mechanism happening near the amine droplet. For this purpose, laminar finite rate model was used where the reaction rate is determined by the Arrhenius expression. This model ignores the effect of turbulent fluctuations on the reaction rates. This makes the model computationally inexpensive. The net source of chemical species i due to reaction is computed as the sum of the Arrhenius reaction sources over the N_R reactions that the species participate in [13] :

$$R_i = M_{w,i} \sum_{R=1}^{N_R} R_{i,r} \tag{7.2}$$

Where, $M_{w;i}$ is the molecular weight of species i and $R_{i,r}$ is the Arrhenius molar rate of creation/destruction of species i in reaction r. Reaction may occur in the continuous phase between continuous-phase species only, or at wall surfaces resulting in the surface deposition or evolution of a continuous-phase species.

For a non-reversible reaction the molar rate of creation/destruction of species i in reaction is given by [33]

$$R_{i,r} = \Gamma\ (v'_{I,r} - v''_{I,r})\ (\ k_{f,r} \prod_{j=1}^{N} [C_{j,r}]^{(njr\ +\ mjr)}\ ) \tag{7.3}$$

Γ represents the net effect of third bodies on the reaction rate. This term is given by

$$\Gamma = \sum_j^N \gamma_{j,r} C_j \tag{7.4}$$

where $\gamma_{j,r}$ is the third-body efficiency of the j^{th} species in the r^{th} reaction

The forward rate constant for reaction r, $k_{f;r}$, is computed using the Arrhenius expression

$$K_{f,r} = A_r\ T^{\beta}\ e^{-E/RT} \tag{7.5}$$

Initially, the amine droplets were introduced evenly at the domain inlet with a mole fraction of 0.1 and the rest of the mixture had carbon dioxide. The reason for this is that the DPM model can only allow the volume of the secondary phase to be 10% to 12% of the primary phase. The second simulation was done with same even distribution of amine droplets at the inlet with the same mole fraction however this time, the carbon dioxide mole fraction was 0.22 while the rest was other combustion gases as is observed in a normal exhaust gases. In both the cases, the amount of carbon dioxide captured by a single droplet was calculated, at the same time the amount of MEA carbamate, which is the main product, was also calculated.

7.2.1Results

1) MEA mole fraction 0.1 and CO_2 mole fraction 0.9

The following figure shows the reduction of CO_2 mole fraction by a single amine droplet.

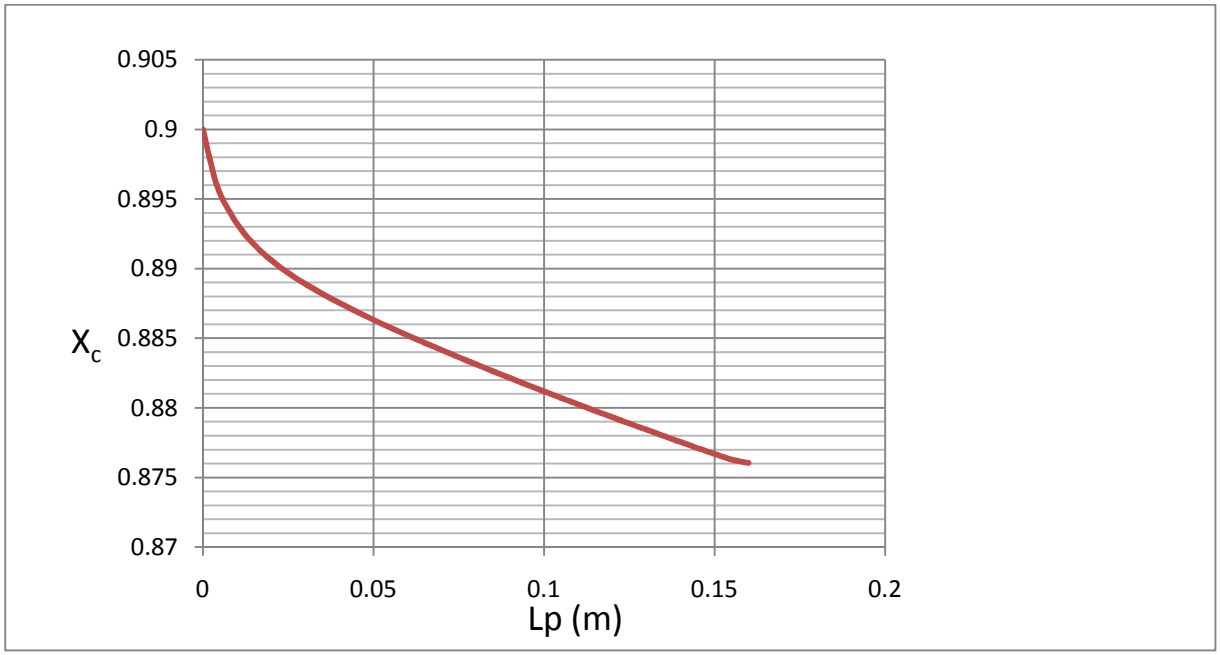

Fig 7.2.1: CO_2 captured by a single amine droplet.

The figure above shows a sharp decrease in the CO_2 mole fraction initially. Then the rate of decrease reduces. This is due to the fact that initially there is no reacted material in the drop so the reaction takes place at the surface of the drop. The reaction itself is the rate determining step but later the rate determining step is the diffusion of CO_2 through the product later that has been formed. As the reaction layer builds up, CO_2 has to diffuse through this layer of reacted material to reach the unreacted core. As the product layer builds up, the diffusion through the product layer becomes the dominant factor in controlling the overall process. Since CO_2 is the only gas, the diffusion of CO_2 through to the surface of the drop is nonexistent. The sharp decrease in the CO_2 mole fraction is due to the fact that a single amine droplet captures CO_2 which is 74 times its weight. This fact illustrated in the simple calculations ahead.

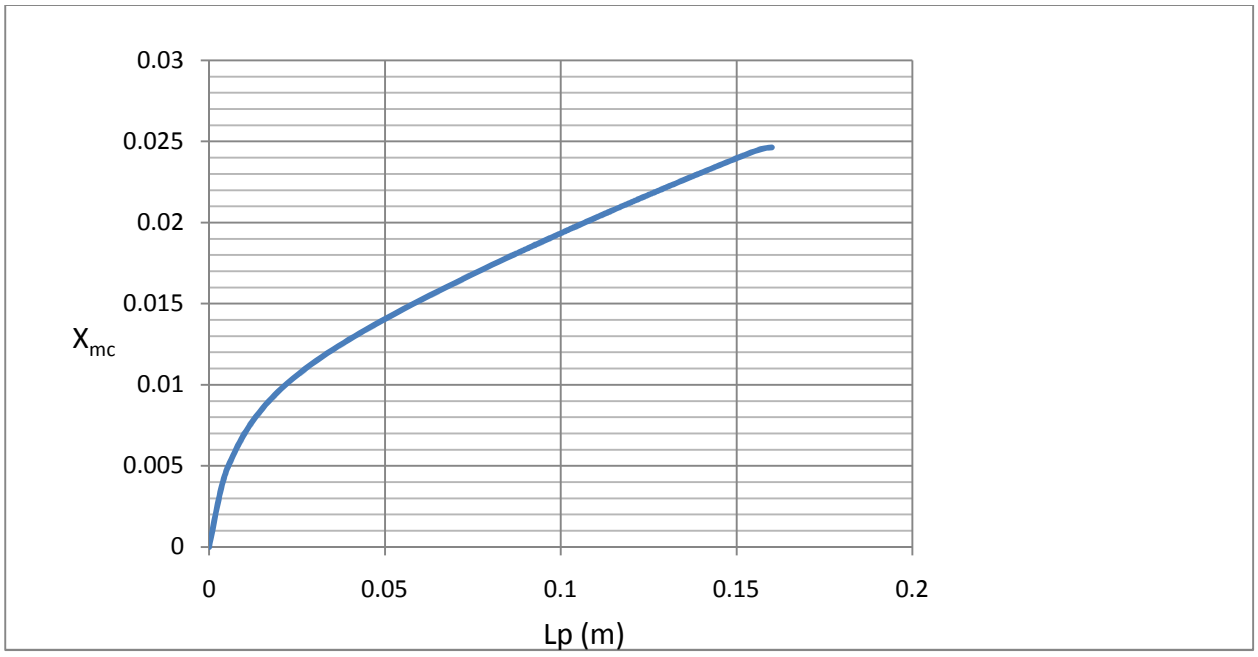

Fig 7.2.2 : MEA carbamate product formation in a single droplet.

The figure above shows the amount of MEA carbamate produced as a result of the reaction in a single amine droplet. Comparison of above two figures shows that the amount of MEA carbamate produced matches exactly with the reduction of CO_2. Here also, the rate of production is steep initially and reduces as the MEA carbamate layer increases.

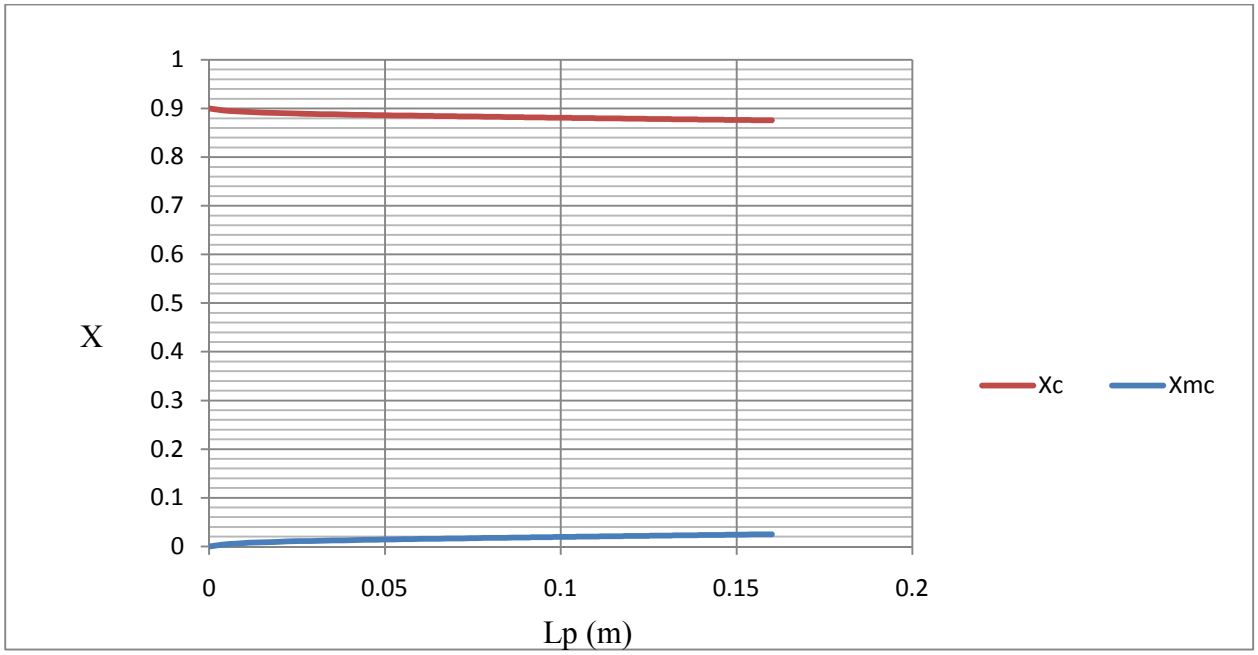

Fig 7.2.3: Drop in CO_2 mole fraction and corresponding increase in the mole fraction of MEA carbamate

Figure 7.2.3 shows that the reduction in CO_2 mole fraction is equal to the increase in the mole fraction of MEA carbamate.

2. MEA mole fraction 0.1, CO_2 mole fraction 0.22 and the other exhaust gases mole fraction 0.68.

Here, a more realistic simulation is done. The CO_2 mole fraction is 0.22 which is normally observed in combustion, while the MEA mole fraction is kept same as before. The other exhaust gases like H_2O, O_2,N_2 and CO constitute the rest of the mole fraction.

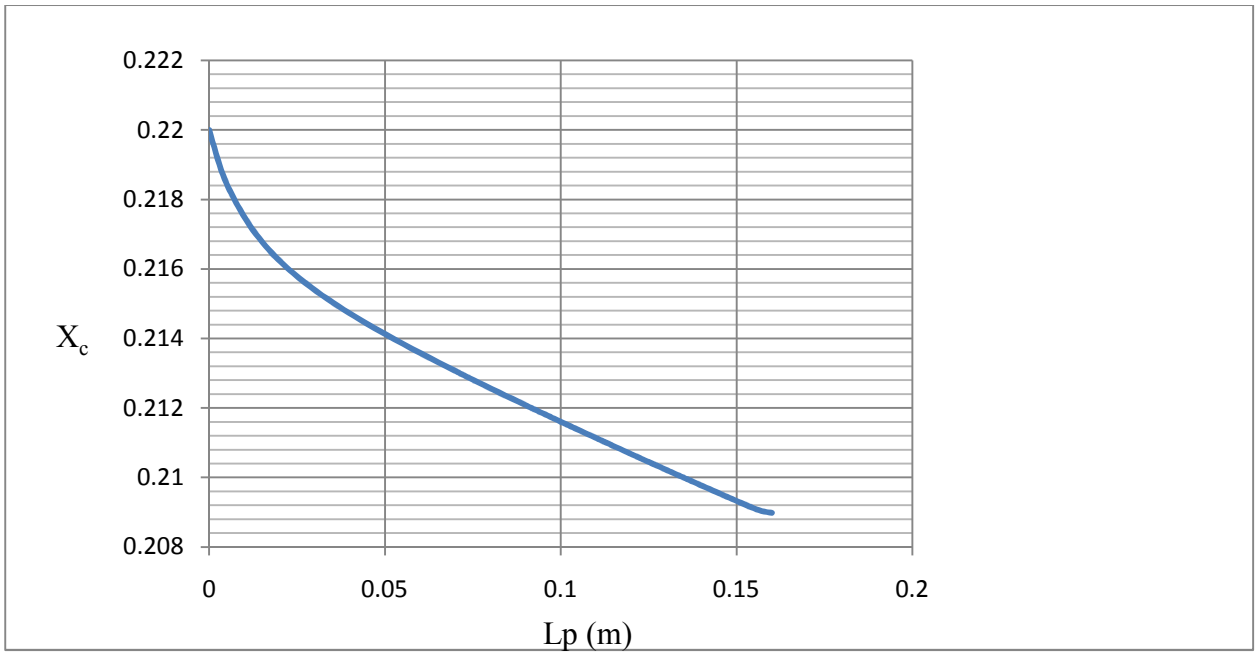

Fig 7.2.4: CO_2 captured by a single amine droplet from exhaust gases

The same trend is seen as before. The rate reduction in CO_2 is more initially and reduces as the process goes on. However, the amount of CO_2 captured here is less than the previous case due to the fact that now CO_2 has to diffuse through other gases towards the surface of the amine droplet.

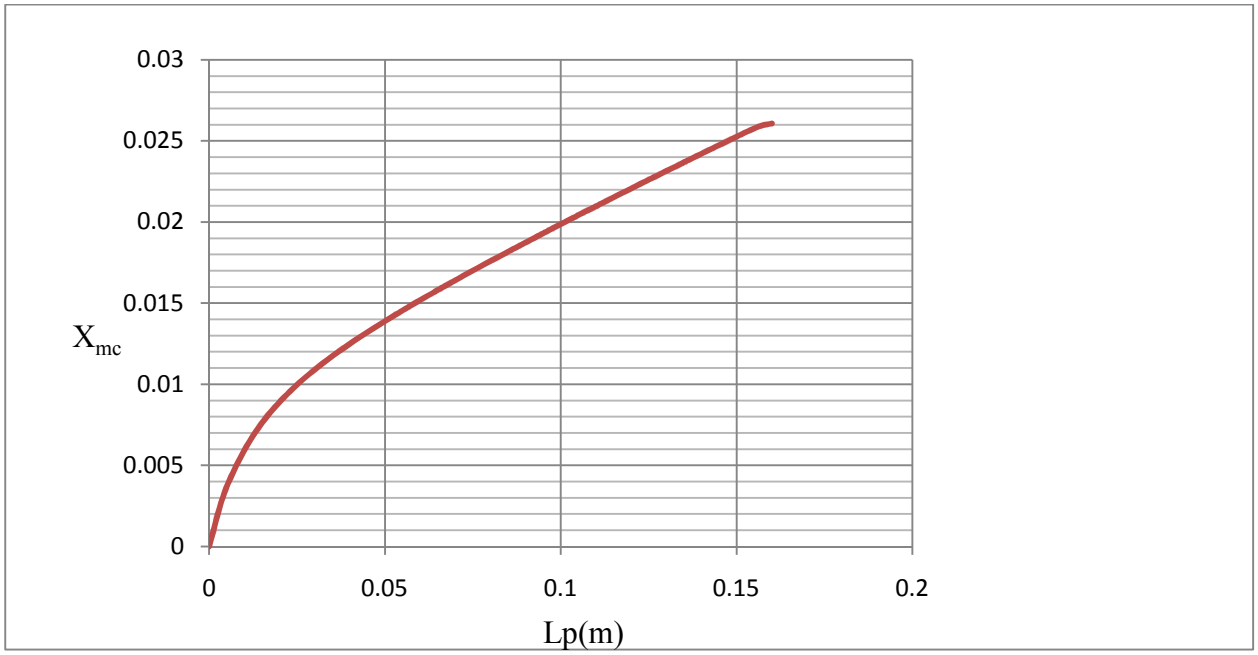

Fig 7.2.5: MEA carbamate product formation in a single droplet.

In Figure 7.2.5, similar trend is observed in the rate of production of MEA carbamate but the amount of carbamte produced is less than the previous case but still it corresponds to the reduction in the CO_2 mole fraction.

7.3 Reaction in Turbulent Regime

The gases in the industrial exhaust chamber are in turbulent flow regime. Hence simulation had to be performed in the turbulent flow regime to make the simulation as realistic as possible. In this case, the size of the domain was 20 m X 20 m X 160 m. A flow velocity of about 1 m/s gives a turbulent flow. In order to simulate the reaction in turbulent regime, Finite Rate/Eddy Dissipation model was used.

This model simulates the reaction according to the Arrhenius equation however also takes into account the effect of turbulent fluctuations affecting the reaction rate.

7.3.1 Results

Here the same pattern is followed as followed in the laminar simulation case. First the simulation with MEA mole fraction of 0.1 and CO_2 mole fraction of 0.9 is done and then the effect of other exhaust gases is incorporated.

1) MEA mole fraction 0.1 and CO_2 mole fraction 0.9

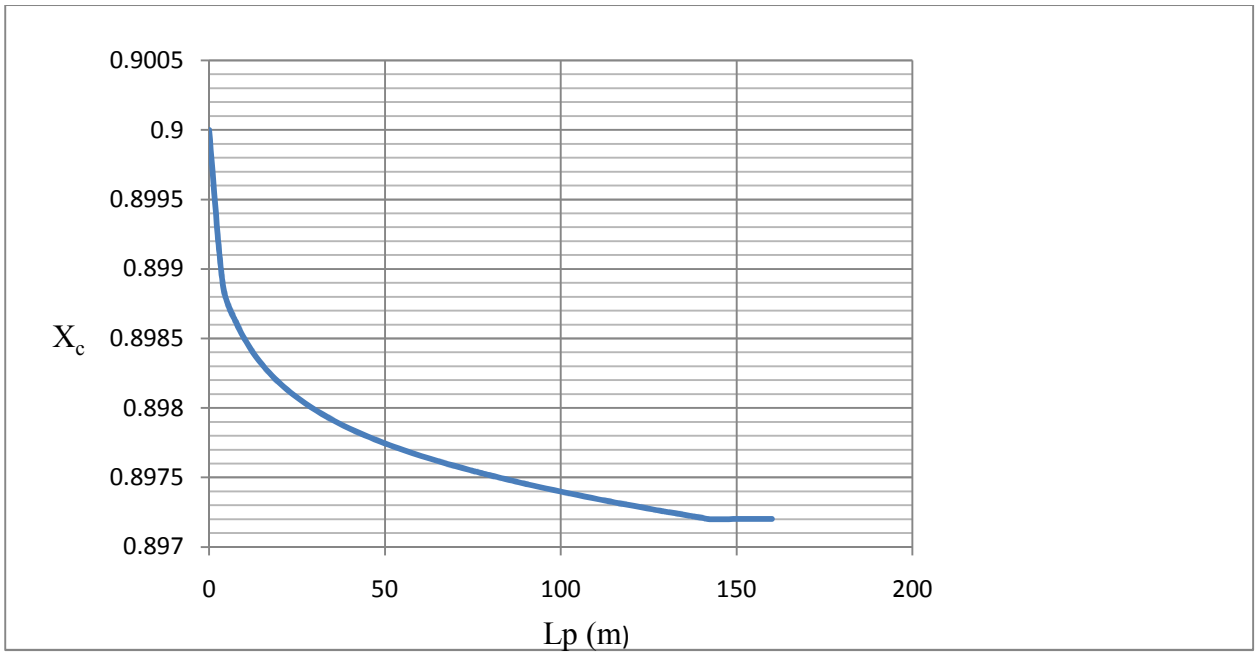

Fig 7.3.1: CO_2 captured by 100 amine droplets.

Figure 7.3.1 shows the same pattern as that observed in the Laminar flow case. Initially the rate of CO_2 decrease is high which reduces as the diffusion through the reacted layer in the drop increases. However the drop of CO_2 initially is much steeper than the one found in laminar case. This can be attributed to the increased level of mixing in the turbulent flow which results in better mass transfer.

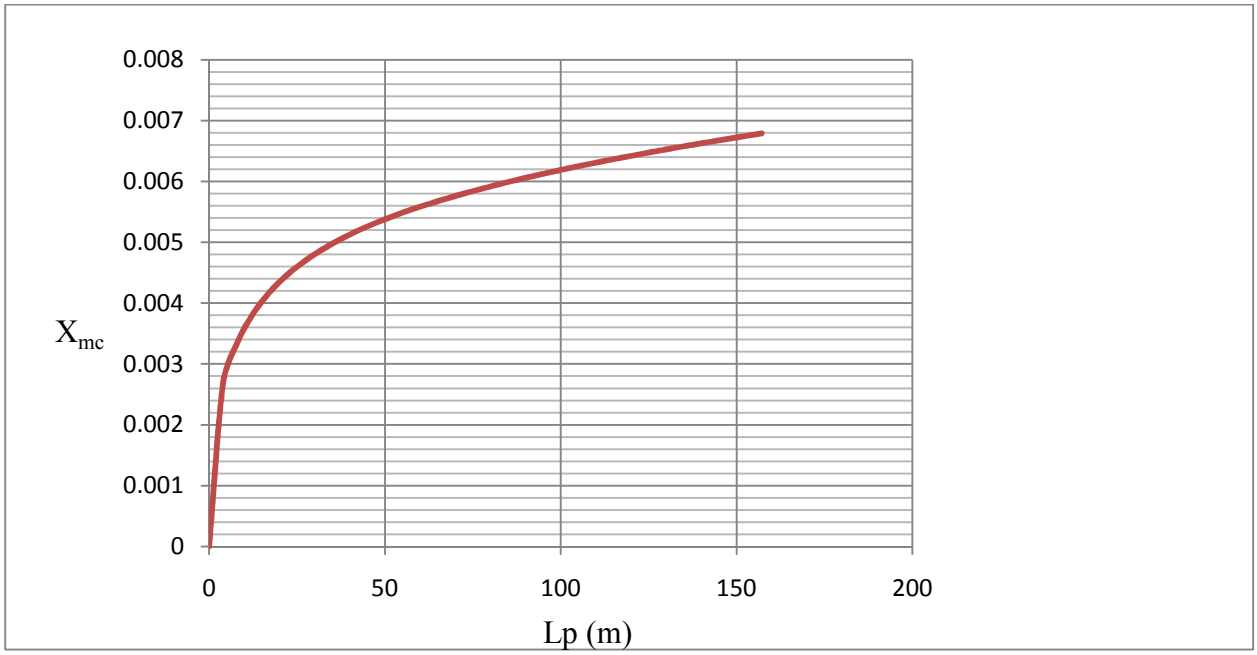

Fig 7.3.2: MEA carbamate product formation 100 amine droplets.

Figure 7.3.2 shows the increase in the MEA carbamate mole fraction which corresponds to the reduction in CO_2 mole fraction. The steep reduction in CO_2 matches with the steep increase in the MEA carbamate mole fraction. The plot indicates that during the time the amine droplet is in the domain, only 0.2% of the amine drop is captures CO_2.

2. MEA mole fraction 0.1, CO_2 mole fraction 0.22 and the the other exhaust gases mole fraction is 0.68.

   This is the most realistic case. Here the effect of other exhaust gases like H_2O, O_2, N_2 and CO is incorporated and the flow is turbulent.

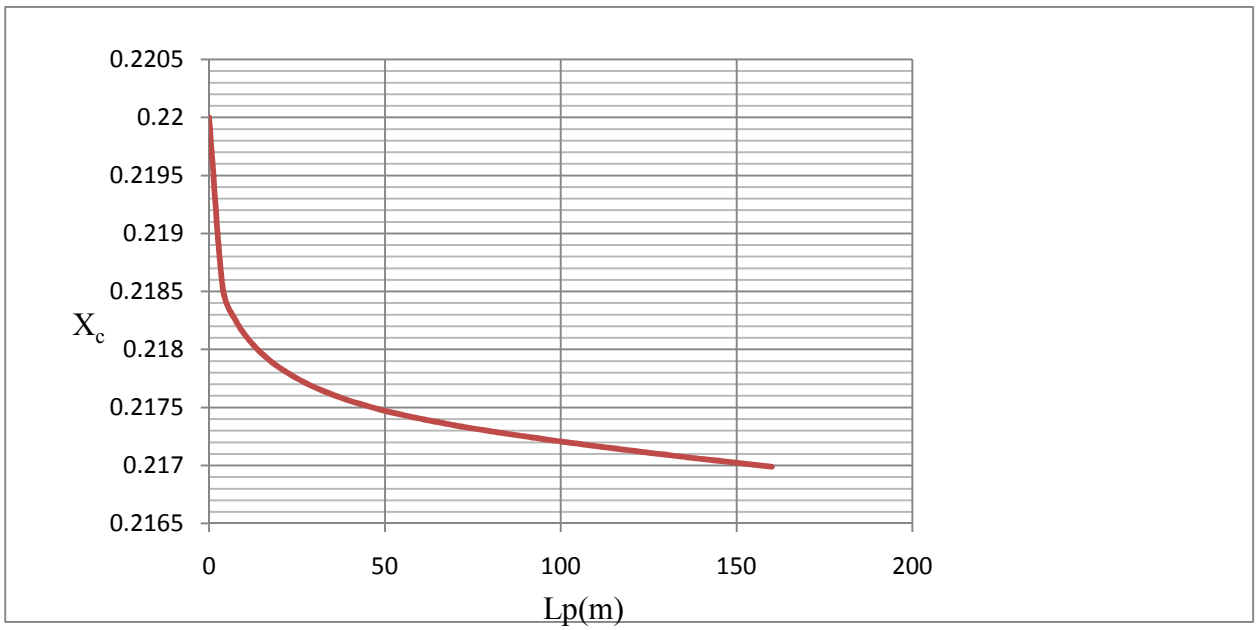

Fig 7.3.3: CO_2 captured by 100 amine droplets from exhaust gases

Figure 7.3.3 shows similar pattern as laminar case with other exhaust gases. Here too the amount of CO_2 captured is less than the case when the other exhaust gases were absent. Here too we can see that there is a sharp decrease in the CO_2 mole fraction initially and later on the rate of capture decreases which is consistent with the shrinking core model. There is a substantial drop in the CO_2 mole fraction as capturing capacity of MEA is 1:73 as mentioned before in laminar case. Here the drop is not as high as in case of laminar simulation as the size of the domain is three orders of magnitude higher than the laminar case but to reduce the computational expense, the MEA mole fraction is kept at 0.1.

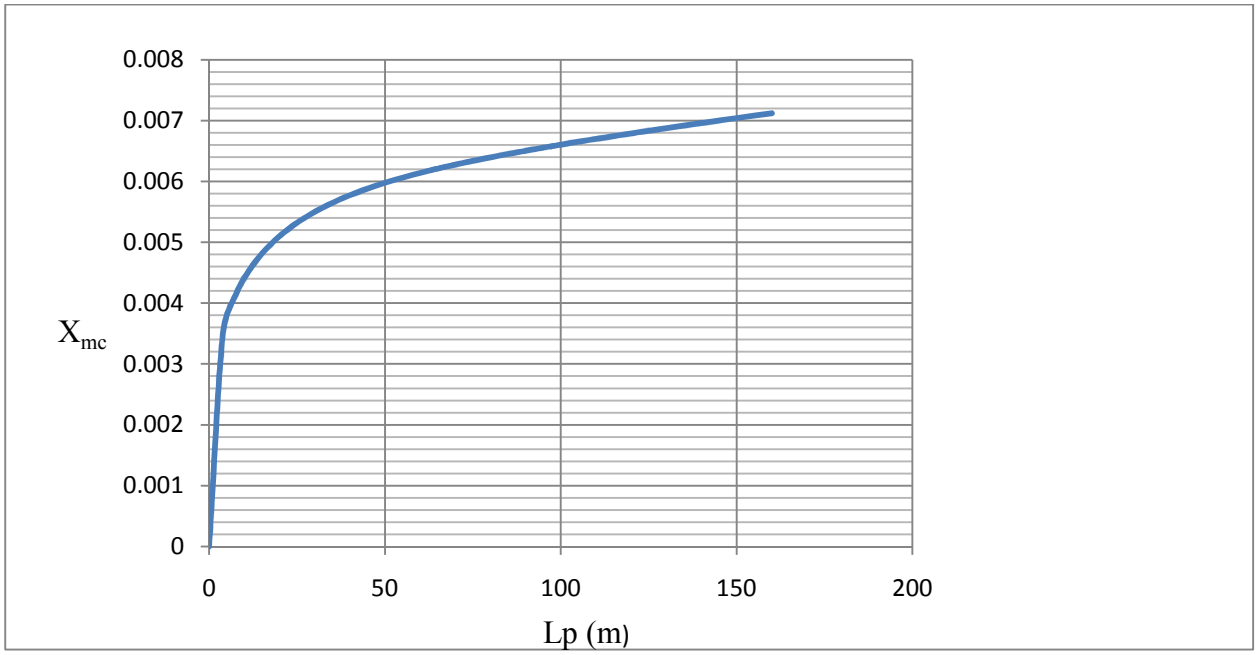

Fig 7.3.4: MEA carbamate product formation 100 amine droplets.

From the plots of the turbulent cases it can be seen that the amount of CO_2 captured is more in the first case than in the second case. The reason for this is that in second case there are other exhaust gases present along with CO_2. Hence CO_2 has to diffuse through these gases to reach towards the amine droplets. However, the pattern of plots of both cases is similar suggesting that initially as there is no reacted material present; CO_2 has no resistance to reaction once it reaches the amine drop. However, later on in the process as the reacted material starts accumulating, CO_2 has to diffuse through this layer to reach to the unreacted material.

7.4 Difference between Laminar and Turbulent simulations

It can be observed from the laminar and turbulent simulations that the amount of CO_2 captured is more in case of laminar simulation than in case of turbulent simulation. In case of reaction in laminar regime, the size of domain is very small as compared to the amount of MEA drops injected. While in

case of turbulent simulation the size of domain increased while the amount of MEA injected remained same. Due to this the CO_2 had to diffuse more to reach MEA.

The flow could have been made turbulent by keeping the same dimensions of the domain as in case of laminar simulation by increasing the velocity. However this is not possible as the velocity of the exhaust gases obtained is very high to be applied in practice. We want the relative velocity of the exhaust gases to be less than the terminal velocity of the MEA drops injected by an atomizer to avoid the loss of MEA to the atmosphere.

In theory the CO_2 in case of turbulent simulation should be more than in laminar case. We can observe this trend by seeing that in turbulent simulation plot the initial curve is very step as compared to that of the laminar simulation plots .This is because in turbulent flow higher level of mixing can reduce the amount of diffusion required by CO_2 to reach MEA. But to achieve this we need to increase the amount of MEA into the domain. Hence multiple injection system is required.

Another important fact to mention is that the MEA utilization is both the laminar cases is same about 2.5% and the same in both the turbulent simulations is 0.75%. This shows that CO_2 can easily diffuse through other exhaust gases and hence the second step of the shrinking core model is not the rate determining step at any time in the process.

7.5 Simple calculations

Presented here are some simple calculations based on the results obtained from the last case, which is turbulent flow with Xmc = 0.1 and Xc = 0.22. Other exhaust gases H_2O, N_2, O_2 and CO constitute the rest of the mole fraction.

The decrease in the mole fraction of CO_2 due to a single amine drop of diameter 300 X 10^{-6} m is 0.002. Now since the molecular weight of CO_2 is 44.01gm/mol, hence one since drop of amine captures

0.088 gm of CO_2. Now the volume of the amine drop is 1.131×10^{-10} m^3 and hence the weight of the MEA drop is 1.144×10^{-7} kg. Hence, it can be predicted that at the same rate the amount of MEA required for capturing 1000 kg of CO_2 is 13.6 kg.

Conclusions

1) From the water evaporation study we can conclude that this process can only be used for primary (MEA) and secondary amines (DEA) but cannot be used for tertiary amines (TEA and MDEA). This is because in case of primary and secondary amines water is not a capturing chemical but a substance needed to complete the second reaction to capture H^+ ions produced as a result of CO_2 capture. In this case, water can be substituted by any base. In case of tertiary amines, water acts as a capture chemical as CO_2 is captured by CO_2 hydrolysis. Due to high water evaporation rate in process of rapid mixing, there is a loss of capturing chemical in case of tertiary amines which will reduce the efficiency of the carbon capturing system.
2) The size of the amine droplets must be kept optimum to increase the surface area available and ensure maximum amine usage.
3) The laminar reaction study proves that a system of carbon capture by rapid mixing is possible without enduring the loss of the amine solution. But since in practice the exhaust gases are in turbulent regime, the turbulent simulations were done which showed encouraging results. The turbulent simulations proved that with proper amine loading conditions and with controlling the velocity of the exhaust gases, effective carbon capture is possible.
4) The turbulence level of the exhaust gases must be controlled to optimum level so that it will reduce the diffusion resistance for CO_2 to reach the amine droplets but should not carry the amine drops with it to avoid loss of amine solution to the atmosphere. For this purpose it must be ensured that the velocity if the exhaust gases must be less than the terminal velocity of the amine drops.

5) The injectors of the amine solution must be spaced out to minimize the loss of energy of the drops by colliding with each other. One way to ensure this is not to have many injectors at the same height. Injectors injecting the amine solution at different height levels can be used. This will also provide for different stages in a carbon capture system.
6) To increase the effectiveness carbon capture system it is important to increase the amount of amine solution injected. As seen in the results of turbulent simulations, the capturing capacity of the turbulent system is better than the laminar system however adequate amount of amine solution must be injected.
7) This thesis proves that carbon capture by the method of rapid mixing is possible resulting in a substantial saving in the cost of contacting mechanisms like membranes and scrubbers.
8) Since the amine drops are free falling while they are capturing the carbon dioxide from the exhaust, collecting the amine solution for the purpose of regeneration is not a problem. Collecting vessels can be placed at the bottom of the capture chamber which can be removed periodically for regeneration.
9) Results of this study conclude that for capturing 1 ton of carbon dioxide, 13.6 kg of MEA with a droplet size of 300 micrometers, will be required.

\

References

1. Joshuah k Stolaroff, David W Keith and Gregory V Lowry; Carbon dioxide capture from atmospheric air via sodium hydroxide spray. *Environ. Sci. Technol.* **2008,** *42,* 2728–2735.
2. Ralph H. Weiland, John C. Dingman, and D. Benjamin Cronin; Heat Capacity of Aqueous Monoethanolamine, Diethanolamine, *N*-Methyldiethanolamine, and *N*-Methyldiethanolamine-Based Blends with Carbon Dioxide. *J. Chem. Eng. Data* **1997,** *42,* 1004-1006
3. R. E. Reitmeierv, . Sivertaznd, H. V. Tartar; Some Properties of Monoethanolamine and its Aqueous Solutions. Chemistry department of University of Washigton.
4. Sanjay Bishnoi, Gary T. Rochelle; Absorption of carbon dioxide into aqueous piperazine: reaction kinetics, mass transfer and solubility. Chemical Engineering Science 55 (2000) 5531-5543.
5. H. Hikita, S. Asai, H. Ishikawa and M. Honda; The Kinetics of Reactions of Carbon Dioxide with Monoethanolamine, Diethanolamine and Triethanolamine by a Rapid Mixing Method. The Chemical Engineering Journal, 13 (1977) 7-12.
6. Thomas A. Hayden, Thomas G. A. Smlth, and Alan E. Mather; Heat Capacity of Aqueous Methyldiethanolamine Solutions. J. Chem. Eng**.** Data 1983, 28, 196-197.
7. B. Hawrylak , R. Palepu , Peter R. Tremaine; Thermodynamics of aqueous ethyldiethanolamine (MDEA) and methyldiethanolammonium chloride (MDEAH+Cl_) over a wide range of temperature and pressure: Apparent molar volumes, heat capacities, and isothermal compressibilities
8. Dow Chemical Database; Properties of Monoethanolamine, 12th edition.

9. Y. Maham, T.T. Teng, L.G. Hepler, A.E. Mather; Volumetric properties of aqueous solutions of monoethanolamine, mono- and dimethylethanolamines at temperatures from 5 to 80 deg C
10. D. Barth, C. Tondre," G. Lappai, and J.-J. Delpuech; Kinetic Study of Carbon Dioxide Reaction with Tertiary Amines in Aqueous Solutions. J. Phys. Chem. 1981, 85, 3660-3667.
11. Leila Faramarzi, Georgios M. Kontogeorgis , Kaj Thomsen, Erling H. Stenby; Extended UNIQUAC model for thermodynamic modeling of CO2 absorption in aqueous alkanolamine solutions
12. Melaku Habte and Savas Yavuzkurt; Simulation of Acoustic Enhancement of heat transfer in a droplet heat exchanger. GT2007-27179, ASME Turbo Expo 2007, May 14-17, 2007, Montreal, Canada
13. Lionel Dubois, Diane Thomas; CO2 Absorption into Aqueous Solutions of Monoethanolamine, Methyldiethanolamine, Piperazine and their Blends. Chem. Eng. Technol. 2009, 32, No. 5, 710–718.
14. Dow chemical Database; Standard state thermodynamic properties at 298.15 k. 12th edition.
15. D. Barth, C. Tondre and J.-J. Delpuech; Kinetics and Mechanisms of the reactions of carbon dioxide with alkanoamines: Adisscussion concerning the cases of MDEA and DEA. Chemical Science Engineering Vol 39, No. 12, pp. 1753-1757, 1904
16. Lars Kucka, Eugeny Y. Kenig, and Andrzej Gorak; Kinetics of the Gas-Liquid Reaction between Carbon Dioxide and Hydroxide Ions. Ind. Eng. Chem. Res. 2002, 41, 5952-5957.
17. Noman Haimour, Ali Bidarian and Orville C. Sandall; Kinetics of the reaction between carbon dioxide and methylaiethanolamine. Chemical Engineering Science. Vol. 42. No. 6, pp. 1393-1398. 1987.

18. Ryszard Pohorecki and Wladyslaw Moniuk; Kinetics of reaction between carbon dioxide and hydroxyl ions in aqueous electrolyte solutions. Chemical Engineering Science, Vol. 43, No. 1, pp. I677 -1684, 1988.
19. Abdalla S. Hanafi, Safaa I. Mahmoud, and Hesham F, Thermal and hydrodynamic characteristics of forced and mixed convection flow through vertical rectangular channels. Thermal Science: Vol. 12 (2008), No. 2, pp. 103-117.
20. Neeraj Kumbhakarna ans Stefhen Thynell; Calculating thermodynamic properties of energetic materials using ab initio quantum chemical methods.
21. Anand V. Patwardhan and Man Mohan Sharma; Kinetics of Absorption of Carbon Monoxide in Aqueous Solutions of Sodium Hydroxide and Aqueous Calcium Hydroxide Slurries. *Ind*. Eng. Chem. Res. 1989,28, 5-9.
22. *Geed* F. Versteeg and Wlm P. M. van SwaaiJ; Solubility and Diffusivity of Acid Gases (CO_2, N_2O) in Aqueous Alkanolamine Solutions. J. Chem. Eng. Data 1988, 33, 29-34.
23. Yadollah Maham, Loren G. Hepler,Alan E. Mather,Andrew W. Hakin and Robert A. Marriott ; Molar heat capacities of alkanolamines from 299.1 to 397.8 K. J. Chem. Soc., Faraday T rans., 1997, 93(9), 1747È1750.
24. INEOS, Gas/ Spec MDEA speciality amine
25. INEOS Gas/Spec MEA speciality amine.
26. Alexey A. Alexandrov; The Equations for Thermophysical Properties of Aqueous Solutions of Sodium Hydroxide. 14th International Conference on the Properties of Water and Steam in Kyoto.

27. Siu-Ming Yih* and Keh-Perng Shen; Kinetics of Carbon Dioxide Reaction with Sterically Hindered 2-Amino-2-methyl-1-p ropanol Aqueous Solutions. Ind. Eng. Chem. Res. 1988,27, 2237-2241.

28. Jerry A Bullin, John C Plasek; The Use of MDEA and Mixtures of Amines for Bulk CO2 Removal. Proceedings of the Sixty-Ninth GPA Annual Convention. Tulsa, OK: Gas ProcessorsAssociation, 1990: 135-139.

29. P. Bhattacharya, A.N. Samanta, S. Chakraborty; Spray evaporative cooling to achieve ultra fast cooling in runout table. International Journal of Thermal Sciences 48 (2009) 1741–1747

30. Octave Levenspiel; Chemical Reaction Engineering. Third Edition

31. Yunus A Cengel; Heat Transfer a Practical Approach; Second Edition.

32. CHEMKIN User Manual.

33. FLUENT User manual.